Available online at www.sciencedirect.com

ScienceDirect

journal homepage: www.elsevier.com/locate/he

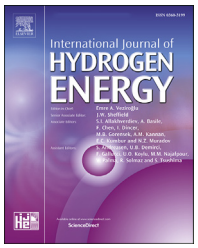

Steam reforming of methanol, ethanol and glycerol over nickel-based catalysts-A review

Sujoy Bepari [a], *Debasish Kuila* [a,b,*]

[a] *Department of Chemistry, Applied Sciences and Technology, North Carolina A & T State University, Greensboro, NC, 7411, USA*

[b] *Department of Nanoengineering, Joint School of Nanoscience and Nanoengineering, North Carolina A & T State University, Greensboro, NC, 27411, USA*

HIGHLIGHTS

- Potential Ni based catalysts for steam reforming of three alcohols (methanol, ethanol and glycerol).
- Textural properties of different Ni-catalysts.
- Comprehensive review on role and performance of Ni-based catalyst for MSR, ESR and GSR.
- Effect of active metal and catalyst support on product distribution and conversion of alcohols.
- Future trend of Ni-based catalyst on steam reforming of three alcohols.

ARTICLE INFO

Article history:
Received 7 May 2019
Received in revised form
24 July 2019
Accepted 1 August 2019
Available online 29 August 2019

Keywords:
Hydrogen
Layered double hydroxides
Mesoporous silica
Mesoporous carbon
Fuel cell
Ni-based catalysts

ABSTRACT

Depletion of non-renewable energy sources such as coal and natural gas is paving the way to generate alternative energy sources. Hydrogen, a very promising alternative energy has the highest energy density (143 MJ/kg) compared to any known fuel and it has zero air pollution due to the formation of water as the only by-product after combustion. Currently, 95% of hydrogen is produced from non-renewable sources. Hydrogen production from renewable sources is considered a promising route for development of sustainable energy production. Steam reforming of renewable sources such as methanol, ethanol and glycerol is a promising route to hydrogen production. This review covers steam reforming of these three alcohols using Ni-based catalysts with different supports. Chemistry of the steam reforming reactions is discussed. Hydrogen yield depends on operating conditions, the nature of active metal and the catalyst support. Supports play an important role in terms of hydrogen selectivity and catalyst stability because of their basic characteristics and redox properties. Synthesis of suitable catalysts that can suppress coke formation during reforming is suggested.

* *Corresponding author*. Department of Chemistry, Applied Sciences and Technology, North Carolina A & T State University, Greensboro, NC, 7411, USA.
E-mail address: .dkuila@ncat.edu (D. Kuila).

https://doi.org/10.1016/j.ijhydene.2019.08.003

Introduction

Increase of worldwide demand on energy and environmental issues are the major concerns of today, in the 21st century [1]. Currently, non-renewable materials such as fossil fuels are the main energy sources. Depletion of fossil fuels and environmental pollution are now triggering attention generating emission-free alternative energy sources. Hydrogen is considered as one of the clean and green energy sources as it produces only water after combustion. Hydrogen has an energy density of 143 MJ/kg, that is three times greater than any liquid hydrocarbon-based fuels [2]. At present, 95% of hydrogen is produced from non-renewable resources such as natural gas and other fossil fuels [3]. Hydrogen production from renewable energy sources is an alternative strategy to overcome the environmental problems.

Some of the major concerns for the use of H_2 as a fuel are its storage and transportation. The use of metal hydrides is a convenient way to store hydrogen; however, the capacity is not enough due to the availability of a material capable of minimizing diffusion and leakage of hydrogen during handling [4]. Thus, on-site production of H_2 is an excellent strategy to avoid its storage problems. There is some application of hydrogen in many fields. Hydrogen has been used by many rocket engines developers around the world. Those are RL10 (Aerojet Rocketdyne- USA), LE-5 (Mitsubishi Japan), HM7B (Snecma- France), YF-73 (CALT- China), KVD-1 (Russia), CE-20 (HAL- India) [5]. There are lot of advantage to use hydrogen as aviation fuel. It eliminates most of the greenhouse gas (GHG) emissions including carbon-based emissions, soot and sulphur oxides [6]. Hydrogen is used in the refining industry as a petrochemical for hydrocracking and desulphurization. In the chemical industry, it is used for ammonia production and fertilizer for agriculture. It has many other applications such as metal production and fabrication, methanol production, food processing and electronic sectors.

Several methods have been developed to produce hydrogen such as water electrolysis, hydrocarbon reforming, photocatalysis and biotechnology [7–9]. Among different methods, catalytic steam reforming of gas, hydrocarbons and alcohols is a promising technology to produce highly purified hydrogen [10–13]. Industrially, methane is used as the main fuel for hydrogen production and other hydrogen carriers may be used for the reaction [14]. The worldwide production of hydrogen comprises mainly 48% hydrogen that is obtained through steam reforming of methane (SRM), while 30% is produced from reforming of naphtha/oil, 18% from coal gasification and 3.9% only from electrolysis [15]. The main drawback of methane steam reforming is that it requires high temperature (800–1000 °C) compared to alcohols [16]. Further, CH_4 is also a non-renewable source. For commercialization of PEMFC, a stable supply of hydrogen is needed. The fuel cell with proton exchange membranes (PEMFC) is one of the most promising systems to generate electricity from hydrogen [17]. PEMFCs are zero-pollutants emission system due to the electrochemical reaction between hydrogen and oxygen and the chemical energy is transferred into clean electrical power [18,19]. The major drawback of PEMFC is that it requires high purity hydrogen because the anodic Pt-based catalyst can tolerate only less than 10 ppm of CO [20]. So, the development of hydrogen production technology from alternative and renewable energy sources has been considered as a very important strategy in recent years [21]. Catalytic steam reforming of renewable alcohols (methanol, ethanol and glycerol) is one of the most promising routes to produce hydrogen for a fuel cell to generate electricity [22]. Methanol is considered as a renewable alcohol as it is produced from renewable sources. It reduces the intensity of fossil fuel as the main feed of methanol plant and reduces CO_2emission. Methanol can be produced from carbon dioxide and hydrogen that can be obtained from electrolysis and employing renewable sources [23]. Methanol formation by CO_2 hydrogenation reaction is shown below:

$$3H_2 + CO_2 \leftrightarrow CH_3OH + H_2O$$

Like methanol, ethanol can be synthesized from renewable resources. In recent years, ethanol is produced from agricultural feedstocks such as corn or sugarcane in the US or Brazil [24]. Ethanol can also be produced from biomass generated from lignocellulosic feedstock. It has clear advantage such as broad availability and low cost of the feedstock.

Glycerol is a main byproduct from biodiesel industry. Biodiesel is produced from vegetable oil (renewable source) and alcohol via transesterification reaction. As biodiesel is produced from renewable source, glycerol is considered as renewable alcohol because it also comes from renewable source.

Methanol has several advantages in the reforming process. It is the simplest alcohol as it contains one carbon atom. Due to the presence of one carbon atom in methanol, it can easily react with steam at low reaction temperature [25].

Methanol is a liquid at room temperature and biodegradable, although it is toxic. It has high hydrogen to carbon ratio [26–28]. Methanol steam reforming (MSR) (Eq. (1)) generally occurs at low temperature (200–300 °C) [14] and the reaction proceeds through multiple steps as shown below. Two side reactions are commonly considered: methanol decomposition (Eq. (2)) and water gas shift reaction (Eq. (3)) [29,30]:

$$CH_3OH + H_2O \leftrightarrow CO_2 + 3H_2 \quad \Delta G_{298K} = -4 \text{ kJ/mol} \tag{1}$$

$$CH_3OH \leftrightarrow CO + 2H_2 \quad \Delta G_{298K} = +25 \text{ kJ/mol} \tag{2}$$

$$CO + H_2O \leftrightarrow CO_2 + H_2 \quad \Delta G_{298K} = -28.606 \text{ kJ/mol} \tag{3}$$

Another feedstock that can be used for hydrogen production, via the steam reforming process, is ethanol. Ethanol has several advantages due to its higher hydrogen content, availability, non-toxicity, handling (it is a liquid at room temperature) and safety issues [31,32]. As in MSR, ethanol steam reforming (ESR) is an endothermic reaction. CO_2 and H_2 are produced during the main reaction (Eq. (4)). Other carbon-containing products such as CH_4, CO, CH_3CHO and C_2H_4 are also formed during the ESR reactions [33–37]. Side reactions such as dehydrogenation (Eq. (5)), decomposition (Eq. (6)) and dehydration (Eq. (7)) of ethanol take place in parallel with the main reaction. The formation of CH_3CHO is basically due to

dehydrogenation of ethanol. C_2H_4 is produced through ethanol dehydration and CH_4 is formed due to ethanol decomposition. While coke formation arises due to ethanol dehydration, ethanol dehydrogenation favors hydrogen production [37]. CO reacts with water through a water-gas shift reaction to produce H_2 (Eq. (3)).

$$C_2H_5OH + 3H_2O \rightarrow 2CO_2 + 6H_2 \quad \Delta G_{298K} = +64\ kJ/mol \quad (4)$$

$$C_2H_5OH \leftrightarrow CH_3CHO + H_2 \quad \Delta G_{298K} = +39.6\ kJ/mol \quad (5)$$

$$C_2H_5OH \leftrightarrow CH_4 + CO + H_2 \quad \Delta G_{298K} = -20\ kJ/mol \quad (6)$$

$$C_2H_5OH \leftrightarrow C_2H_4 + H_2O \quad \Delta G_{298K} = +8.4\ kJ/mol \quad (7)$$

Steam reforming of glycerol is also carried out at higher temperature as in the case of EtOH. One of the attractive reasons for using glycerol stems from its availability. 100 kg of glycerol is produced per ton of biodiesel production via transesterification (Scheme 1) of edible or non-edible oil [38,39].

An increase in worldwide production of biodiesel has led to an increase in production of crude glycerol [40]. However, the cost of production of biodiesel is quite high. To minimize the cost on production the by-product glycerol has become quite important for production of valuable products such as hydrogen via steam reforming. Glycerol steam reforming (GSR) is relatively a new method to produce hydrogen [39]. GSR is an endothermic reaction (Eq. (8)). There are several side reactions such as glycerol decomposition (Eq. (9)), steam reforming of methane (Eq. (10)) and water gas shift reaction (Eq. (3)) that always occur along with the main reaction [41].

$$C_3H_8O_3 + 3H_2O \leftrightarrow 3CO_2 + 7H_2 \quad \Delta G_{298K} = -49.51\ kJ/mol \quad (8)$$

$$C_3H_8O_3 \leftrightarrow 3CO + 4H_2 \quad \Delta G_{298K} = +37.49\ kJ/mol \quad (9)$$

$$CH_4 + 2H_2O \leftrightarrow CO_2 + 4H_2 \quad \Delta G_{298K} = +113.298\ kJ/mol \quad (10)$$

Carbon formation during steam reforming process is the main issue on catalyst deactivation. Ethylene polymerization (Eq. (11)), 'Boudouard' reaction (Eq. (12)) and methane decomposition (Eq. (13)) [42–44] are responsible for coke formation.

$$C_2H_4 \rightarrow Polymers \rightarrow Coke \quad (11)$$

$$2CO \leftrightarrow CO_2 + C \quad \Delta G_{298K} = -120\ kJ/mol \quad (12)$$

$$CH_4 \leftrightarrow 2H_2 + C \quad \Delta G_{298K} = +51\ kJ/mol \quad (13)$$

The standard Gibbs free energy changes were taken from a book [45].

Different catalysts based on noble (Rh, Ru, Pt, Pd) and non-noble (Ni, Cu) metals have been used for steam reforming of alcohols. Among them, Ni catalyst has shown promising activity to facilitate the C-C bond cleavage in reforming reactions [46–48]. It is quite cheap and used industrially but suffer deactivation in long term operations due to coke formation [49]. However, the addition of Ce and Pr oxides to Ni catalyst system can diminish the coke formation [50,51]. This review focuses on the development of Ni-based catalysts for steam reforming of three alcohols: methanol, ethanol and glycerol. The performance of the catalysts for each alcohol is described in the sections below. The catalyst for other reforming reactions such as partial oxidation, dry reforming and autothermal reforming processes are not considered in this review.

Methanol steam reforming

Many researchers have investigated Ni-based catalysts activity based on different parameters such as preparation, addition of promoters and calcination and reduction temperatures of the catalysts.

Ni-based catalysts

The activity of nickel-based catalysts depends on its physical properties. High surface area with adequate nickel dispersion along with small particle size are the key factors for the synthesis of highly active catalysts. The physical properties of different catalysts reported in literature are shown in Table 1.

Table 1 shows different Ni based catalysts with different supports prepared for methanol steam reforming reactions. Abrokwah et al. [22] synthesized Ni-MCM-41 catalyst by one-pot hydrothermal method. The catalyst exhibit type-IV

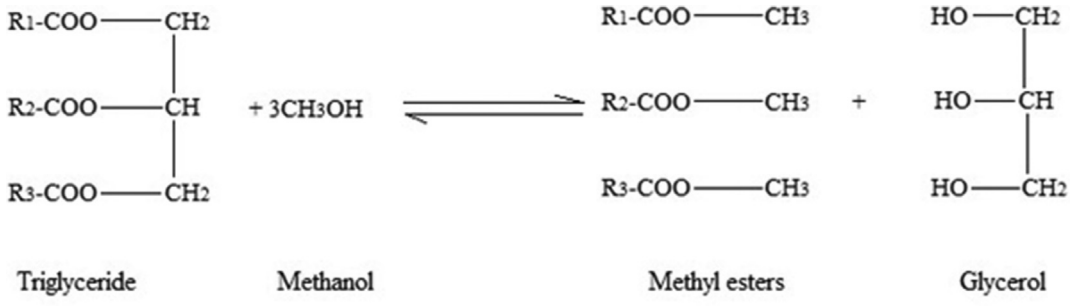

Scheme 1 – Transesterification reaction for production of biodiesel.

Table 1 – Physical properties of different Ni-catalysts reported in literature.

Catalyst	Preparation method	S_{BET} (m^2/g)	Pore size (nm)	Pore Volume (cm^3/g)	Reference
Ni-MCM-41	OPHM	824.6	3.8	0.84	[22]
Ni/CeO_2-MgO-Al_2O_3	IMP	78	7.0	0.19	[49]
$NiSn/CeO_2$-MgO-Al_2O_3	IMP	75	6.9	0.18	[49]
Ni/CeO_2-MgO-Al_2O_3	PM	75	6.4	0.16	[49]
$NiSn/CeO_2$-MgO-Al_2O_3	PM	86	6.4	0.18	[49]
Cu-Ni/DND	IMP	230	25	–	[52]
CuNiZnAl	COP	93	17	–	[53]
CuNiAl	COP	113	10	–	[53]
γ-Al_2O_3	–	223.9	5.4	0.30	[54]
$10Ni/Al_2O_3$	IWMP	162.1	6.1	0.25	[54]
$10La\text{-}5Ni/Al_2O_3$	IWMP	132.0	7.0	0.23	[54]
$10La\text{-}7.5Ni/Al_2O_3$	IWMP	122.2	6.7	0.20	[54]
$10La\text{-}10Ni/Al_2O_3$	IWMP	114.3	7.0	0.19	[54]
$10La\text{-}12.5Ni/Al_2O_3$	IWMP	111.9	7.3	0.20	[54]
$10La\text{-}10Ni/SiO_2$	IWMP	227.3	13.6	0.74	[54]
10La-10Ni/MgO	IWMP	11.9	29.4	0.09	[54]
MoC	ICM	10.2	–	–	[55]
NiMoC	ICM	19.3	–	–	[55]
$Cu\text{-}Ni/TiO_2$	IMP	98.2	22.41	0.59	[56]
$10Ni\text{-}TiO_2$	FOS	309.8	3.32	0.203	[57]
NiAl	COP	201.6	5.08	0.48	[58]
NiAl-Au	COP	195.0	3.95	0.41	[58]
NiAl-Rh	COP	213.2	3.72	0.38	[58]
NiAl-Ir	COP	215.8	3.72	0.39	[58]
Ni_{10}-Al	IMP	84	53	0.73	[59]
Ni_7Cu_3-Al	IMP	78	58	0.77	[59]
Ni_5Cu_5-Al	IMP	82	55	0.71	[59]
Ni_3Cu_7-Al	IMP	78	58	0.78	[59]

OPHM: One-pot hydrothermal method, IMP: Impregnation method, IWMP: Incipient Wet impregnation method, COP: Co-precipitation method, ICM: In-situ carburization method, FOS: Facile onestep synthesis, PM: Polyol method.

hysteresis loop in BET studies. The monolayer of N_2-adsorbate was found in the range of relative pressure (P/P_0) 0–0.2. The range between 0.2 and 0.4 is attributed to the capillary condensation of N_2 in the MCM-41 framework. The steepness of the step ($P/P_0 = 0.2–0.4$) suggested that narrow ordered pore size distribution of MCM-41 framework. After addition of metal, the steepness of the BET isotherm curve decreased. This suggests some loss of ordered structure.

Bobadilla et al. [49] prepared Ni based catalysts, such as Ni_3Sn intermetallic compound, by polyol and impregnation methods. All catalysts exhibit type IV nitrogen adsorption-desorption isotherms with H_3-type hysteresis loop (Fig. 1). The surface area increases for the polyol method. However, catalyst surface area slightly decreases upon addition of Sn during the impregnation method. They also reported that both methods were successful to produce nanoparticles although the formation of the spinel structure after metal impregnation depends on the calcination temperature. Nanoparticles produced by polyol method were very sensitive to the temperature of thermal treatment. The H_3 type loop corresponds to pore system formed by a complex structure of interconnected pores with different shapes and sizes. Surface area decreased with addition of Sn. So, the total volume decreased and pore size slightly increased.

Lytkina et al. [52] prepared Cu-Ni/DND (detonation nanodiamonds) catalyst by an impregnation method. The specific surface area was determined based on dispersion of the carbon support. Average particle size obtained from BET analysis is essentially equal to average carbon size particles. The specific surface area was determined based on dispersion degree of the carbon support. Average particle size, mainly the carbon particle size, was obtained using the BET method.

Ni based layer double hydroxides were synthesized by a co-precipitation method [53]. The surface area decreases after addition of zinc. They reported that the addition of nickel may develop mesoporous structures which provide a large surface area. The pore size was increased due to incorporation of Zn by co-precipitation method. So, the surface area increased.

Ni based catalysts with different supports (Al_2O_3, MgO and SiO_2) were also used for methanol steam reforming studies [54]. Incipient wet-impregnation method was used to synthesize the catalysts. Incorporation of La in the catalysts decreased the specific surface area of Ni/Al_2O_3 catalyst. This indicates that La entered into mesoporous channels and blocked some of the pores. The surface area decreases continuously with an increase of Ni loading. The adsorption-desorption curves for catalysts (Al_2O_3, $10Ni/Al_2O_3$, $10La\text{-}10Ni/Al_2O_3$) were broad and nearly horizontal despite narrow pore size distribution centered at 3.3 nm, 3.8 nm (Fig. 2 (inset)), respectively. The results suggest that the materials contained mesopores with an inter-communicating porous network. Due to addition of La by incipient wet-impregnation method, the pore size shifted from 3.3 nm to 3.8 nm and they blocked some pores.

Ni on molybdenum carbide, shown in Table 1, was prepared by an in-situ carburization method [55]. The surface area increases approximately two times after incorporation of Ni. This increment might suggest lower reduction potential of

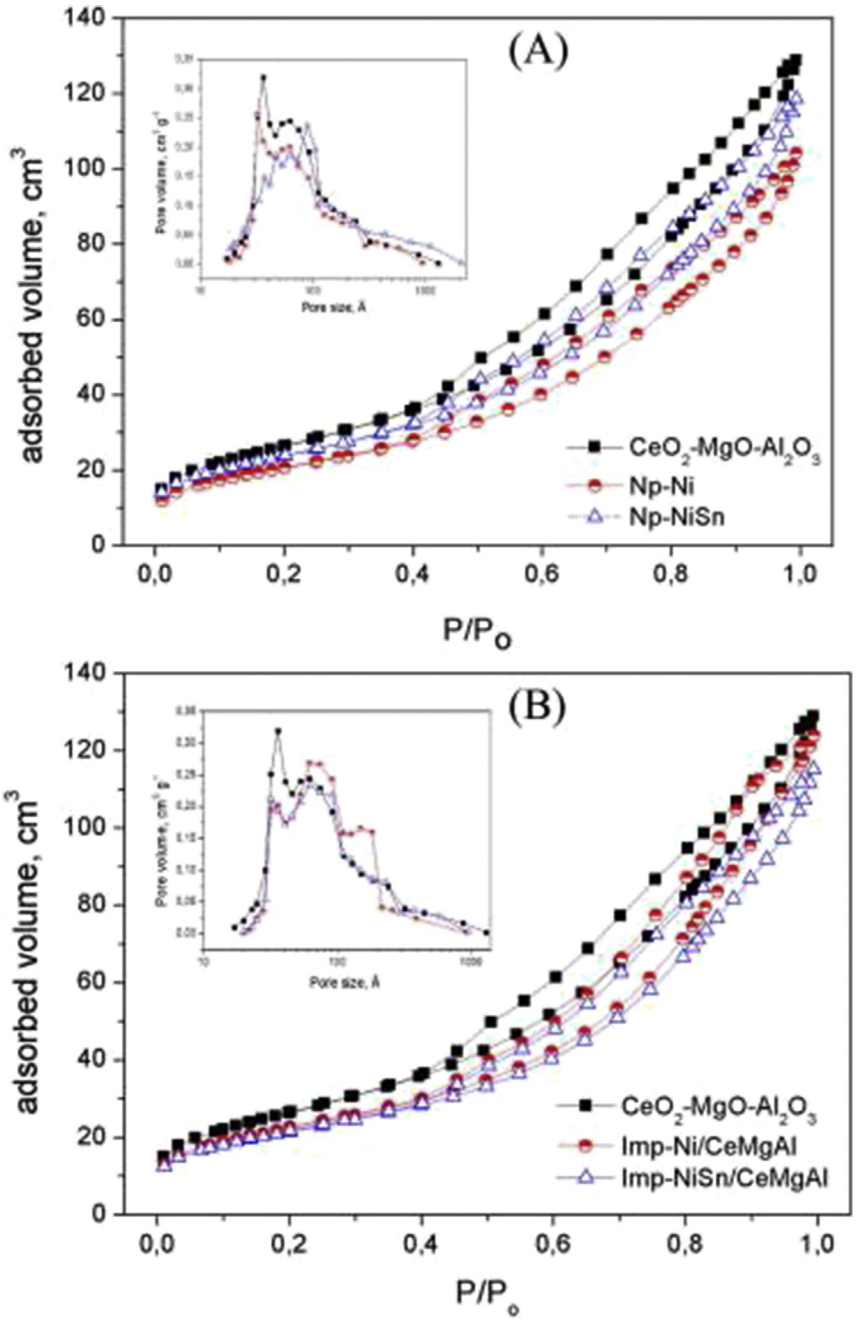

Fig. 1 – BET nitrogen adsorption/desorption isothermal plots of polyol-based catalysts (A) and impregnated catalysts (B). The inset shows the mesoporous particle size distribution plot obtained using BJH method. Reprinted with permission from Ref. [49].

MoO_3 after addition of Ni. The particle size from BET technique was determined by the mobility of the metal ions. The mobility was limited by low reduction temperature, which leads to smaller particle size and higher surface area.

Impregnation method was also utilized to prepare Cu-Ni/TiO_2 catalyst [56]. The catalyst exhibits BET hysteresis loop between the relative pressure (P/P_0) 0.4 to 0.9 and suggests that capillary condensation occurs in the mesopores. They observed a noticeable hysteresis loop, similar to type-IV, at high relative pressure. All catalysts generally showed H1 (uniform size and shape) type hysteresis loops and correspond to slit-like pores. The specific surface area and total pore volume decreased due to addition of Ni. However, the pore size increased. These results suggested that the smaller pores were blocked first, which increased the average pore size.

Deshmane et al. [57] prepared Ni on mesoporous TiO_2 catalyst by facile one step synthesis method. They observed a hysteresis loop associated with the BET isotherm that can be attributed to capillary condensation. The BET analysis suggests that a mesoporous structure is present in the catalyst. This result is quite similar to that observed by Tahay et al. [56]; H2 type hysteresis loop was observed for TiO_2. However, after Ni incorporation, the hysteresis loop changed from H2 to H4. This reflected the significant change in the textural properties.

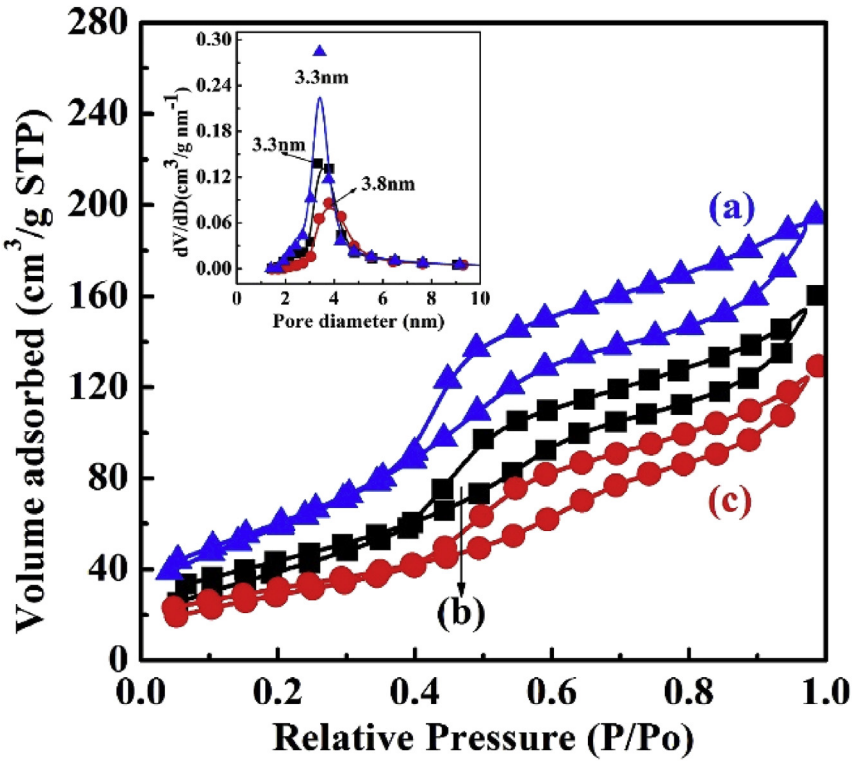

Fig. 2 – BET N_2 adsorption-desorption isotherms of: (a)Al_2O_3, (b)10Ni/Al_2O_3 and (c)10La-10Ni/Al_2O_3 catalysts. Reprinted with permission from Ref. [54].

Depending on metal ions, the pore size and pore volume varied.

Another mesoporous structure such as Ni-M-Al (M = Au, Rh and Ir) layer double hydroxides (LDH) catalysts were synthesized by a co-precipitation technique [58]. All the catalysts have high surface area. Smaller pore diameter and volume were obtained after incorporation of M^{3+} into the NiAl-LDH framework. Smaller pore diameter and pore volume were obtained after addition of noble metals. Similarly, Ni_{10}-Al catalyst and that modified with Cu were prepared by an impregnation procedure [59]. All the catalysts have type-IV isotherms with hysteresis loop, indicating the formation of mesoporous materials like Ni-M-Al catalysts [58]. The BET plots reveals negligible pore volumes and BJH results suggest that all the catalysts have an average pore diameter of 55 nm. The lower surface area and pore volume were obtained due to metal incorporation [59]. Incorporation of Ni/Cu might block the Al_2O_3 pores during impregnation method.

Activity of different nickel-based catalysts for methanol steam reforming

In this section, the activity of the different nickel-based catalysts is discussed. A summary of the activity of the catalysts is shown in Table 2.

Liu et al. [60] obtained 100% methanol conversion over Ni/CeO_2 catalyst at 400 °C. The oxygen vacancy created on ceria surface helps water dissociation and metal support interaction which facilitated the transfer of oxygen between ceria and Ni. This oxygen might be helpful for oxidation reaction and responsible for high methanol conversion and selectivity to H_2 at high temperature. They proposed a methanol steam reforming reaction mechanism as shown below. They suggested that the reactions occurred over the Ni sites or at the Ni-ceria interface:

$$\text{HCOO-(a)} \rightarrow \text{H(a)} + CO_2\,(g), \text{ or HCOO-} + \text{O (lattice)} \rightarrow CO_3^{2-} + \text{H (a)} \rightarrow CO_2\,(g) + \text{O (lattice)} + \tfrac{1}{2}\,H_2\,(g) \quad (14)$$

A small amount of methoxy species (CH_3O) is formed and facilitated the undesired reactions.

$$CH_3O(a) \rightarrow CO\,(a) + 3H\,(a) \rightarrow C^0/Ni_3C + 3/2\,H_2\,(g) \quad (15)$$

$$C^0/Ni_3C + 2O\,(\text{lattice})/OH \rightarrow CO_2 + Ni^0 + H_2\,(g) \quad (16)$$

It was reported that Ni is the only metal that is involved in the above reactions. Metal support interactions played an important role to complete the reaction cycle. The H_2/CO ratio increased with the increase of Ni content initially. However, it decreased at higher Ni loading. It reflects that more Ni content decreases the catalyst activity and lowers H_2 production. The Ni content more than 5 wt% favors decomposition reaction more than steam reforming and the reverse water gas shift reaction.

Bimetallic catalyst such as Cu-Ni/Al_2O_3 with different compositions were also tested for methanol steam reforming by Khzouz et al. [61]. The reactions were carried out in the temperature range of 225–325 °C with steam/carbon ratio of 1.7 and liquid hourly space velocity of 0.77 h^{-1}. They obtained maximum methanol conversion at 325 °C. Methanol conversion decreases from 94% to 90% with the increase of

Table 2 – Ni-based catalyst activity for methanol steam reforming.

Catalyst	X_{CH3OH} (%)	Temperature (°C)	S_{H_2} (%)/H_2 yield	S_{CO} (%)/CO yield	S_{CO_2} (%)/CO_2 yield	H_2/CO	Reference
Ni/CeO_2	100	400	–	–	99	–	[60]
$5Ni\text{-}5Cu/Al_2O_3$	98.5	325	2.2	0.6	0.35	3.67	[61]
$3Ni\text{-}7Cu/Al_2O_3$	97	325	1.8	0.65	0.3	2.77	[61]
$7Ni\text{-}3Cu/Al_2O_3$	98.5	325	2.0	0.7	0.2	2.86	[61]
2Ni5ZnAl	95	500	–	4	–	–	[62]
2NiAl	10	500	–	30	–	–	[62]
4Ni10ZnAl	97	500	–	6	–	–	[62]
4NiAl	30	500	–	29	–	–	[62]
8Ni20ZnAl	100	500	–	2.5	–	–	[62]
8NiAl	60	500	–	40	–	–	[62]
NiAl	16.1	340	73.4	6.4	20.2	11.47	[58]
NiAl	35.0	380	73.6	4.6	21.8	16	[58]
NiAl-Au	27.1	280	66.1	28.9	5	2.29	[58]
NiAl-Au	82.9	340	60.5	29	5	2.09	[58]
NiAl-Au	99.4	380	36.2	1.6	26	22.63	[58]
NiAl-Rh	36.7	280	63.4	35.4	0.6	1.79	[58]
NiAl-Rh	80.2	340	37.7	8.7	20.0	4.33	[58]
NiAl-Rh	82.6	380	32.2	0.3	26.1	107.33	[58]
NiAl-Ir	44.6	280	62.5	35.5	0.4	1.76	[58]
NiAl-Ir	85.3	340	46.9	20.9	9.3	2.24	[58]
NiAl-Ir	92.9	380	40.1	0.3	25.7	133.67	[58]
$10Ni/Al_2O_3$	100	500	80	2.7	24	29.63	[54]
$10La\text{-}10Ni/Al_2O_3$	100	500	85	2.5	22.5	34	[54]
$10La\text{-}10Ni/SiO_2$	100	500	80	5	17.5	16	[54]
10La-10Ni/MgO	100	500	79	5	20	15.8	[54]
$Cu\text{-}Ni/TiO_2$/monolith	83.8	225	85.8	8.8	–	9.75	[56]
$Cu\text{-}Ni/TiO_2$/monolith	92.6	300	92.7	9.6	–	9.66	[56]
Ni-MCM-41	45.1	350	99.9	99.0	0.9	1.01	[22]
Ni/MoC	97	350	70	5	20	14	[55]

temperature from 225 °C to 275 °C for 7%Cu-3%Ni catalyst. There is a slight increase of water conversion within 225–275 °C. The water conversion decreases rapidly in the range of 300–325 °C, indicating that the increase of water conversion was part of the methanol steam reforming reaction. Other bimetallic catalysts such as 5%Cu-5%Ni and 3%Cu-7%Ni showed an increase of methanol conversion with increasing reaction temperature. This result indicates that methanol decomposition might have occurred on the catalyst surface.

Men and Yang [62] prepared NiZnAl catalysts with different metal loading for MSR reaction. They found that methanol conversion and CO selectivity were strongly dependent upon catalyst composition and catalytic properties. The catalytic properties changed with the Ni and Zn loading. Ni catalyst without Zn showed less activity in the reforming reaction. Methanol conversion increases with the increase of metal loading and it suppresses the undesired side reaction (CO production). The full conversion was achieved with 8Ni20ZnAl catalyst at 500 °C and weight hourly space velocity (WHSV) of 40.68 h^{-1}. Qi et al. [58] investigated NiAl LDH catalyst with and without noble metals (Au, Rh and Ir) for MSR studies. They used integrated-membrane reactor for MSR in the temperature range of 300–400 °C. Methanation reaction is favored upon addition of noble metals at high temperature. So, formation of CH_4 reduced the H_2 yield. H_2/CO ratio increased with reaction temperature for all catalysts. H_2 production increased a little for NiAl-LDH catalyst. After incorporation of noble metals (Au, Rh and Ir), the ratio of H_2/CO increased with the increase of temperature. It is due to CO production that decreased drastically at higher reaction temperature (380 °C).

Lu et al. [54] synthesized Ni on different supports (Al_2O_3, SiO_2, MgO) modified by La. The reactions were carried out between 300 and 600 °C (Fig. 3). H_2 selectivity increased after the addition of La. Other products selectivity decreased due to the presence of La in the catalyst. The highest H_2/CO ratio was achieved for $10La\text{-}10Ni/Al_2O_3$ catalyst. The ratio decreased due to change of support, because it increased the CO selectivity.

Tahay et al. [56] prepared Cu-Ni catalyst on different supports (TiO_2 and monolith) for MSR reactions in a fixed bed reactor. The catalyst supported onTiO_2 gave promising results in terms of H_2 and CO selectivity over monolith catalyst. However, changing the support from TiO_2 to mesoporous silica has a significant effect on conversion and selectivity of MSR reactions. The selectivity of H_2 and CO increased with the increase of temperature. So, the H_2/CO ratio was also increased.

Ni-MCM-41 catalyst, synthesized by one-pot hydrothermal procedure [22], showed 45.1%conversion of methanol at 350 °C. This catalyst favored the CO selectivity and it was not suitable for water gas shift reaction (WGSR). The H_2 and CO selectivity were almost same for Ni-MCM-41 catalyst. So, the H_2/CO ratio was 1.01. This result suggested that Ni selectively produced CO.

Ni/MoC catalyst was also prepared for methanol steam reforming reaction [55]. Catalyst shows good activity in terms of higher methanol conversion and hydrogen yield after Ni

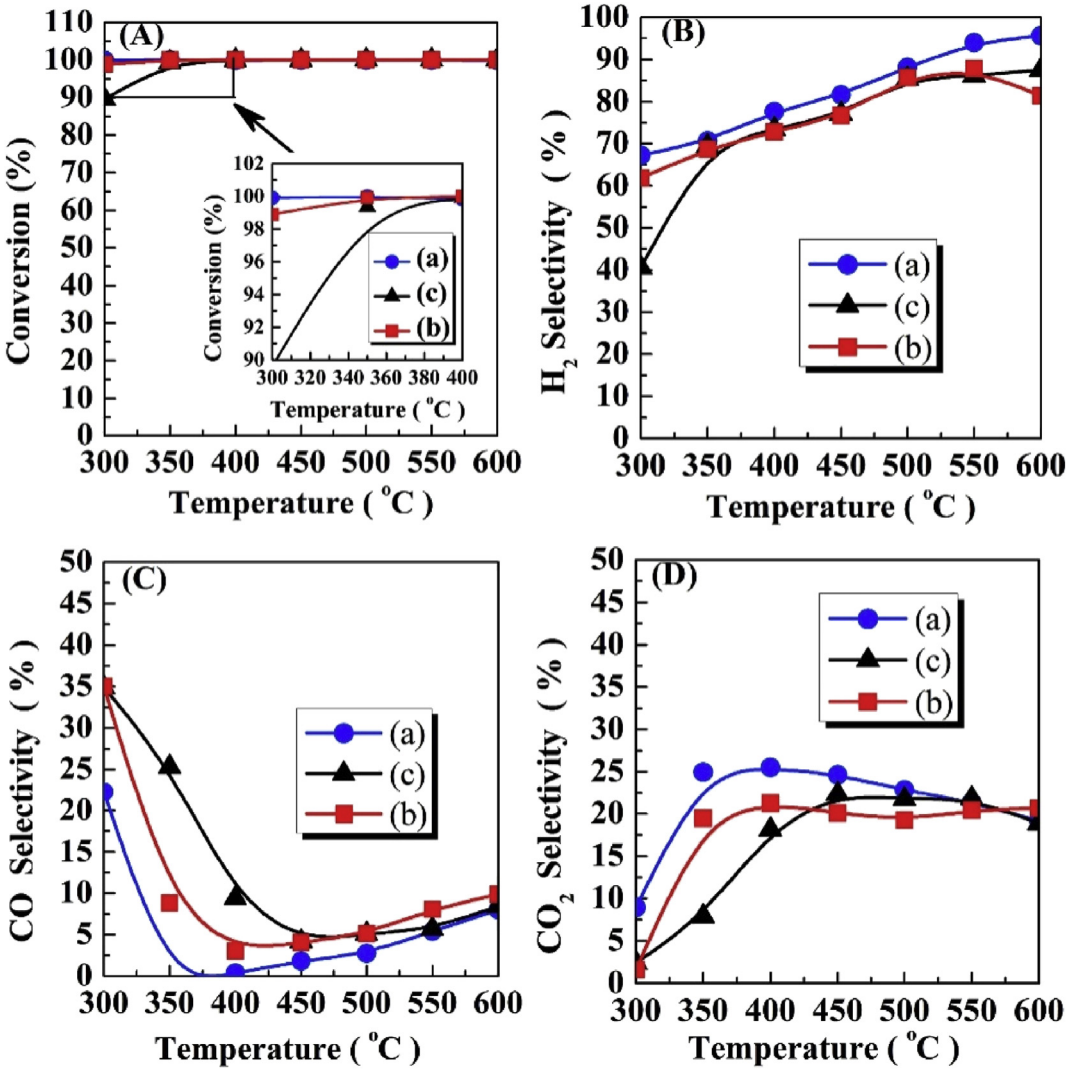

Fig. 3 – Effect of temperature on (A) CH_3OH Conversion, (B) H_2 selectivity, (C) CO selectivity and (D) CO_2 selectivity over (a) 10La-10Ni/Al_2O_3, (b) 10La-10Ni/SiO_2 and (c) 10La-10Ni/MgO. Reprinted with permission from Ref. [54].

incorporation. The reaction was carried out in the temperature range of 200–400 °C. The highest conversion was achieved at 350 °C. H_2 yield was more than CO yield due to addition of Ni on MoC support. So, the H_2/CO ratio was high.

Chemistry of methanol steam reforming

Several mechanisms have been described and there is some agreement in the research community. The production of H_2 basically happens due to methanol decomposition (Eq. (2)) and water gas shift reaction (Eq. (3)) [63–66]. As per the mechanism, CO concentration is higher than the equilibrium concentration. Another mechanism deals with the formation of methyl formate intermediate [67].

$$2CH_3OH \rightarrow HCOOCH_3 + 2H_2$$

$$HCOOCH_3 + H_2O \rightarrow CH_3OH + HCOOH$$

$$HCOOH \rightarrow H_2 + CO_2$$

At first, methanol dehydrogenates to produce methyl formate and hydrogen. Then the methyl formate reacts with water to give methanol and formic acid. After that, formic acid is decomposed to form CO_2 and H_2. In this mechanism, CO is not formed by methanol decomposition, which reflects that its formation due to the water gas shift reaction (Eq. (3)).

The other mechanism described two active sites: one for MSR (Eq. (1)) and water gas shift reaction (Eq. (3)) and another for methanol decomposition reaction [68].

Cu based catalysts are mainly used in methanol steam reforming (MSR). However, some researchers used Ni based catalysts for MSR. The effect of different parameters such as metal loading, calcination temperature and preparation method on the catalysts textural property is discussed. Many Ni based catalysts are mesoporous materials. Different types of isotherms are obtained based on the effect of those parameters. The catalyst activity in terms of methanol conversion and product distribution is reported. Finally, the chemistry of MSR reactions is discussed.

Ethanol steam reforming (ESR)

Metal catalysts play an important role on ethanol conversion and hydrogen production in ethanol steam reforming (ESR). Both noble (Rh, Ru, Pt, Pd, Ir, La) and non-noble metals (Ni, Co) were used in ESR reactions [69–75]. These metals are able to break the high energy C-C bond which is an important characteristic of these catalysts for ethanol conversion [69–75]. Despite the active metal, the supports also interact with ethanol and effect its conversion or transformation to other products [43]. The support-metal interface is considered as active sites for the reaction of C-C and C-H bonds [76]. Several characteristics of the catalyst surface are required for ethanol conversion during the steam reforming reactions [43]. These characteristics are: (i) break the C-C bonds to form CO/CO_2 and CH_4 rather than C-O activation; (ii) transform the C_1 intermediates to H_2 and CO_2; (iii) activate water/oxygen to suppress the coke deposition.

Ni-based catalysts

Ni catalysts are commonly used for ESR due to their low cost compared to noble metals. The physical properties of some of the Ni based catalysts are shown in Table 3.

Ni on different supports were synthesized by an incipient wet impregnation method [77]. The mesoporous structure was confirmed from pore size of the catalysts. The surface area of HTc-type structure increases after calcination [89]. When compared with other catalysts, Cu promoted Ni-Co/HTc structure shows high surface area. Han et al. [78] prepared Cu-Ni-Al_2O_3-ZrO_2 xerogel catalysts with different Cu loading. All catalysts exhibit type-IV isotherms. The pores shrink during conventional drying. Thus, the ink-bottle shaped pores were formed during sample preparation. The isotherm exhibited larger adsorption volume at higher pressure region, indicating that catalysts had high mesoporosity. The surface area of the catalysts increased with the increase of Cu loading. Higher dissociation rate of hydrated Cu^{2+} ions might be the cause to increase the surface area. In the condensation process of hydrated ions, H_2O was the leaving group, Cu^{2+} shows higher condensation rate than Ni^{2+} and Al^{3+} ions [79,80].

Single step evaporation induced self-assembly (EISA) method was also used to prepare a dual templated Ni-Al_2O_3 catalyst for ESR reaction [81]. Both catalysts exhibit type-IV isotherm and H1-type hysteresis loop (Fig. 4(a)) and the catalysts retain a mesoporous structure with uniform pore distribution [90]. This result is similar to that reported by Han et al. [78]. Fig. 4(b) shows the pore size distributions for both catalysts. P123-templated Ni-Al_2O_3 catalyst (SNA) showed the monomodal distribution at 10 nm. Other P123 and ionic liquid templated Ni-Al_2O_3 catalyst (SINA) depicted a major distribution centered at 10 nm and minor distribution centered at 3 nm. Mesopores around at 10 nm was due to compound micelles of block copolymer with ionic liquid and mesopores around at 3 nm was due to the individual micelles of ionic liquid.

Ni-Mg-Al catalyst was prepared by a co-precipitation method [82]. Ni-Mg-Al hydrotalcite catalyst exhibits high surface area as shown in Table 3. Surface area decreases with the impregnation of ceria. This was due to the clogging of the pores by cerium oxide [91]. Ni-doped ordered mesoporous carbon (NiOMC) was synthesized by EISA method [83]. The catalyst exhibits type-IV isotherm, indicating the presence of a mesoporous structure. Similar kind of structure was obtained by Han et al. [78]. Ramirez-hernandez et al. [84] prepared Ni/Al catalyst by sol-gel method. In addition, with an increase of yttrium loading, the surface area and pore volume decrease because of thermal sintering and the inclusion of metal particles into the support pores.

Prasongthum et al. [85] observed 10NiSP (Nickel on silica porous) catalyst exhibits type IV isotherms with H1-type hysteresis loop in the relative pressure range (P/P_0) of 0.07–1.0. This result confirms the typical characteristics of mesoporous structure with cylindrical pores [92]. The shape of the isotherm of 10NiSF (Nickel on silica fiber) is linear with relative pressure of P/P_0 of 0, indicating that the catalyst is a non-porous material. Small surface area corresponds to non-porous material [93]. After deposition of Ni, the surface area increases up to 5 m^2/g due to Ni covered the support surface [93]. Surface area decreases with the increase of Ni loading for NiCNTs-SF. This was due to the blockage of pores by the Ni particles [94]. Ni on SBA-15 catalyst was synthesized by Rodriguez-Gomez and Caballero [86]. The surface area decreases with the increase of Ni loading. The catalysts were prepared by deposition precipitation method. The channel structure of the SBA-15 was preserved even though the surface are decreased and fibrous structures of phyllosilicate phases were obtained after the treatment [95–97]. Ni/Mg/Al catalysts with different Mg loading was prepared by Li et al. [87]. All the catalysts were synthesized by a co-precipitation method. NiMg10Al catalyst exhibits the lowest surface area among all catalysts. Specific surface area increased with the increase of Mg loading up to 8 wt%. Then, it decreased.

NSAZ-Ae (Ni-Sr-Al_2O_3-ZrO_2-Aerogel) and NSAZ-Xe (Ni-Sr-Al_2O_3-ZrO_2-Xerogel) catalysts were synthesized by Song et al. [88]. Aerogel catalyst shows higher surface area and pore diameter compared to xerogel catalyst after calcination process. This indicates that well-structured mesopore was maintained by supercritical drying. The gel structure was suppressed by effective removal of solvent molecules [98]. Both catalysts showed type IV isotherms, where capillary condensation occurred in pore [88]. NSAZ-Ae showed H1 hysteresis loop and NSAZ-Xe depicted H2 hysteresis loop. The H2 hysteresis loop resulted ink-bottle neck shaped structure [90,99]. These two types of hysteresis loops arise due to different drying methods utilized during the preparation process.

Activity of different nickel-based catalysts used for ethanol steam reforming

Ni based catalysts were widely used in ethanol steam reforming reactions. Some of the catalytic activity results are shown in Table 4.

Kumar et al. [100] studied the activity of Ni/ZSM-5 catalyst from 450 °C to 650 °C for ethanol steam reforming (ESR) studies. They obtained highest hydrogen selectivity and complete ethanol conversion at 600 °C. They observed some amount of acetaldehyde formed at a low temperature level. H_2

Table 3 – Physical properties of different Ni-based catalysts used for ethanol steam reforming.

Catalyst	Preparation method	S_{BET} (m^2/g)	Pore size (nm)	Pore Volume (cm^3/g)	Reference
Ni/Al_2O_3	IWMP	44.53	3.581	0.29	[77]
Ni/MgO	IWMP	25.41	2.332	0.13	[77]
NiSn/HTc-type material	IWMP	102.4	10.67	0.43	[77]
Cu-Ni-Co/HTc type material	IWMP	136.2	16.84	0.65	[77]
CNAZ	SG	246	6.5	0.40	[78]
0.1CNAZ	SG	247	7.3	0.45	[78]
0.2CNAZ	SG	276	6.1	0.42	[78]
0.3CNAZ	SG	283	6.7	0.48	[78]
1.0CNAZ	SG	295	6.2	0.45	[78]
SNA	EISA	168	11.6	0.49	[81]
SINA	EISA	212	10.8	0.57	[81]
Ni-Mg-Al	COP	11.50	5.278	0.019	[82]
5%Ce/Ni-Mg-Al	IMP	8.15	6.424	0.009	[82]
10%Ce/Ni-Mg-Al	IMP	5.64	9.114	0.007	[82]
NiOMC	EISA	156	3.5	0.73	[83]
NiOMC-R 400	EISA	118	3.4	0.62	[83]
Ni/Al	SG	245	12.4	0.64	[84]
Ni/Al-5Y	SG	204	7.0	0.34	[84]
Ni/Al-10Y	SG	165	8.5	0.33	[84]
Ni/Al-15Y	SG	148	9.6	0.35	[84]
SF	SG	3	12.5	0.001	[85]
10NiSP	IMP	240	11.8	1.170	[85]
10NiSF	IMP	5	7.4	0.013	[85]
5NiCNTs-SF	IMP	152	10.9	0.362	[85]
10NiCNTs-SF	IMP	132	10.7	0.245	[85]
10Ni/SBA-15	DP	283	10.3	–	[86]
8Ni-2Co/SBA-15	DP	272	11.1	–	[86]
5Ni-5Co/SBA-15	DP	261	12.0	–	[86]
2Ni-8Co/SBA-15	DP	269	10.3	–	[86]
NiMg6Al	COP	177	11.8	0.43	[87]
NiMg8Al	COP	212	14.3	0.48	[87]
NiMg10Al	COP	157	12.6	0.42	[87]
NSAZ-Ae	SG	385	13.7	1.35	[88]
NSAZ-Xe	SG	279	8.0	0.56	[88]

SG: Sol-gel method, IMP: Impregnation method, IWMP: Incipient Wet impregnation method, COP: Co-precipitation method, DP: Deposition precipitation method, EISA: Single-step evaporation-induced self-assembly method.

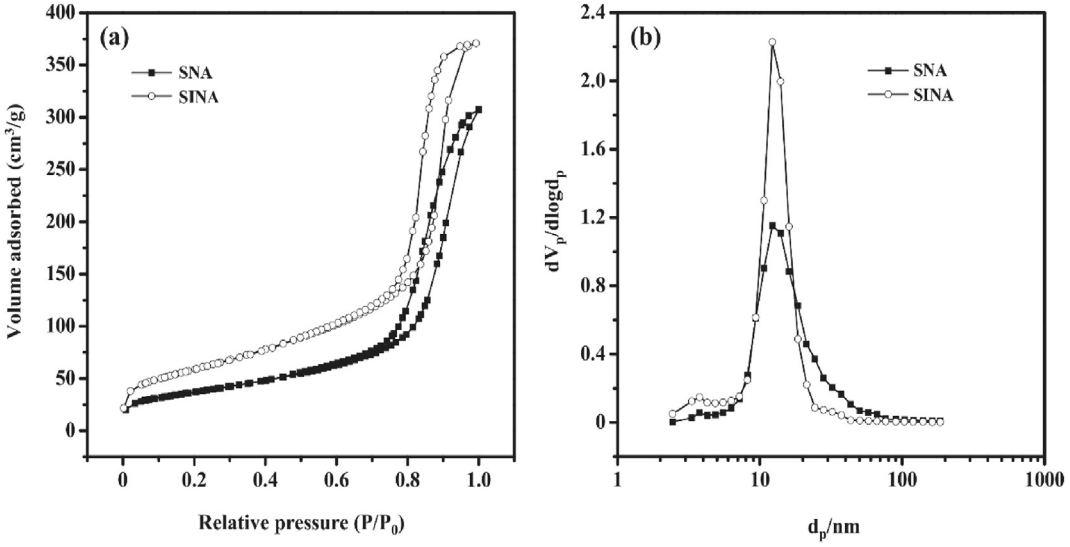

Fig. 4 – (a) N_2 adsorption-desorption isotherm, (b) pore-size distributions of dual templated Ni-Al_2O_3 catalysts. Reprinted with permission from Ref. [81].

Table 4 – Ni-based catalysts activity for ethanol steam reforming.

Catalyst	$X_{C_2H_5OH}$ (%)	Temperature (°C)	S_{H_2}(%)/H_2 yield	S_{CO} (%)/CO yield	S_{CO2} (%)/CO_2 yield	H_2/CO	Reference
Ni/ZSM-5	100	600	75	20	28	3.75	[100]
$LaMgNi_1$	100	600	78	10	12	7.8	[101]
$LaAlNi_1$	100	600	71	10	18	7.1	[101]
10Ni-βzeolite	96	550	78	2	18	39	[102]
10Ni-mβzeolite	95	550	78	1	20	78	[102]
12%Ni/TiO_2	53.77	500	37.48	0.87	12.80	43.08	[103]
12%Ni/20%MMT-TiO_2	83.78	500	51.68	1.29	20.21	40.06	[103]
Ni/Al	100	450	100.1	5.1	55.3	19.62	[104]
Ni/Al-0.05La	100	450	108.7	8.3	62.4	13.09	[104]
Ni/Al-0.1La	100	450	124.3	8.9	63.9	13.97	[104]
Ni/Al-0.15La	100	450	117.9	10.4	61.8	11.34	[104]
Ni/Al-0.2La	98.9	450	64.1	12.3	58.9	5.21	[104]
15Ni/$Ce_{0.7}Pr_{0.3}O_2$	100	450	65	2	20	32.5	[105]
10NiSP	100	500	30	30	40	1	[85]
10NiSF	100	500	47	20	55	2.35	[85]
5NiCNTs-SF	99	500	32	20	49	1.6	[85]
10NiCNTs-SF	99	500	50	28	52	1.79	[85]
10%Ni-W/Al_2O_3	100	600	68.53	14.34	7.79	4.78	[106]
30%Ni-W/Al_2O_3	100	600	69.94	15.76	10.52	4.44	[106]
Ni/CeSmO	100	550	60	22	43	2.73	[107]

selectivity was more than CO selectivity due to addition of Ni on ZSM-5 support. So, the H_2/CO ratio was high.

$LaMgNi_1$ catalyst was used by Aguero et al. [101]. They obtained the highest hydrogen selectivity at temperature 600 °C. They reported that ethanol steam reforming is a sequential reaction [34,108]. Acetaldehyde and hydrogen forms through dehydrogenation of ethanol (Eq. (5)). Acetaldehyde may further convert to acetone and hydrogen. Acetone can be polymerized to give coke. In other context, acetaldehyde, acetone and coke reacted with water to give methane, CO and H_2. Other reactions such as methane steam reforming (Eq. (10)) and water gas shift reaction (Eq. (3)) also occurred simultaneously with ESR. H_2 yield increased due to incorporation of Mg compared to Al. As a result, the H_2/CO ratio decreased a little bit. This result reflected that the presence of Mg favors ethanol steam reforming reaction.

Ni/β m zeolite and Ni/β zeolite with varying Ni loading were tested in ESR studies [102]. 10% Ni loading shows promising activity in respect of H_2 yield and ethanol conversion. They found that the coke formation for Ni/β m zeolite was less compared to the other zeolite. This catalyst was more stable compared to Ni/β zeolite in terms of time-on-stream study. So, coke deposition depends upon the structure and morphology of the catalyst. The hierarchical zeolite (β m zeolite) support showed good activity in ESR. CO selectivity was reduced for mesoporous β zeolite. So, the H_2 to CO ratio increased. This means that intracrystalline mesopores had a great influence on catalyst properties. The selectivity was reduced due to water gas shift reaction (Eq. (3)).

Fig. 5(A),(B) shows the variation of H_2 yield and ethanol conversion with reaction temperature. H_2 yield and conversion increases with temperature for both catalysts. But at higher temperature, in the range from 550 to 600 °C, H_2 yield decreases. 10Ni-MBeta (G) catalyst shows better activity than 10Ni-MBeta (N) at low temperature region. Wang et al. [102] concluded that difference in activity of two catalysts was the method of loading active metal during synthesis.

Other Ni based supported catalysts such as 12% Ni/TiO_2 and 12%Ni/20%MMT-TiO_2 were synthesized for ethanol steam reforming [103]. The MMT (montmorillonite clay) supported catalyst shows good catalytic activity in terms of high ethanol conversion and H_2 yield. The increase in the formation of CH_4 decreased the CO yield due to addition of MMT in the catalyst. The methanation reaction decreases the H_2 and CO yield [109]. Methanation reaction is favored at high temperature due to specific structure of MMT. Methane can also be converted to carbon and H_2 [110]. The addition of MMT created more active site with efficient Ni dispersion. So, the catalyst activity increased and H_2 to CO ratio decreased.

Ni/Al with different La-loaded xerogel catalysts were prepared by Song et al. [104]. Among all the catalysts, Ni/Al-0.1La shows good activity in terms of hydrogen yield and ethanol conversion. All the catalyst exhibits complete ethanol conversion except Ni/Al-0.2La xerogel catalyst. Catalyst without La produced some ethylene. This ethylene was produced mainly from dehydration of ethanol over acid sites of Al_2O_3 [111]. They reported that ethylene formation was suppressed due to addition of La. The H_2/CO ratio decreased with the increase of Ni loading. H_2 and CO production increased with increasing La loading up to 0.15 wt%. However, at higher 0.2 wt% loading, H_2 production decreased and CO production increased.

Hong et al. used a different support to prepare Ni/$Ce_{0.7}Pr_{0.3}O_2$ catalyst for ESR studies by varying Ni loading from 1 to 15% [105]. The 15Ni/$Ce_{0.7}Pr_{0.3}O_2$catalyst shows the highest activity in the ESR studies. They reported that the addition of Pr into ceria favored the generation of oxygen vacancy, which can increase the anti-carbon deposition property. Another advantage of Pr addition was an increase in incorporation of some nickel ions into ceria lattice, thus increasing the interaction between nickel and the support. This also helped to improve anti-sintering property of Ni metal. H_2 selectivity was more than CO selectivity for 15Ni/$Ce_{0.7}Pr_{0.3}O_2$ catalyst. So, the H_2/CO ratio was high.

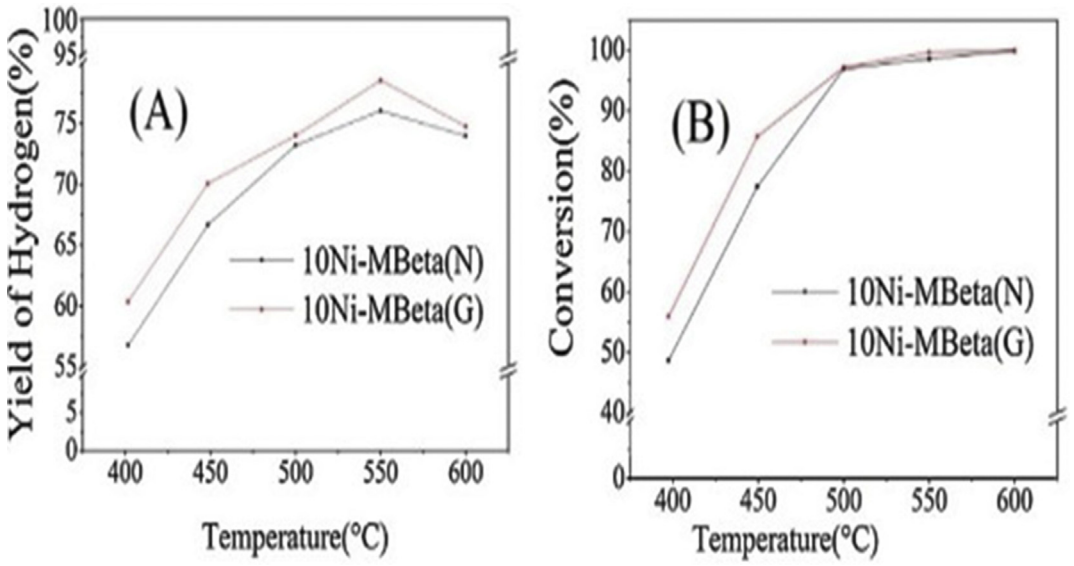

Fig. 5 – Effect of temperature on performance of Ni-catalysts prepared by different loading methods: (A) Yield of hydrogen, (B) Conversion of ethanol (Reaction conditions: 1 atm, S/C = 6:1,0.1 g, 0.075 ml/min) in ethanol steam reforming. Reprinted with permission from Ref. [102].

NiSP (Nickel on porous silica), NiSF (Nickel on silica fiber) and carbon nanotube (CNTs) added to NiSF were used in ESR studies by Prasongthum et al. [85]. Nickel loading was also varied. 10NiCNTs-SF shows good catalytic activity in terms of ethanol conversion and hydrogen yield. They found acetaldehyde and trace amount of ethylene as Ni metal was weaker to break the C-C bond at lower temperature. When the reaction temperature increases, the selectivity of acetaldehyde, ethylene and methane decreases. Methane selectivity decreases due to methane steam reforming occurring at higher temperature [112]. The unique characteristics of CNTs with large area of π-electron could help in coke gasification and facilitated the catalyst regeneration. In comparison of all catalysts, 10NiSF showed the highest value of H_2/CO ratio. This is due to less CO production.

Ni-W/Al_2O_3 catalyst with varying Ni loading (10% and 30%) were tested between temperature of 300–600 °C by Hernandez et al. [106]. 30% Ni based catalyst shows better activity in ESR. The presence of Ni favors to form active sites and help to rupture the C-C and C-H bonds [113,114]. The H_2/CO ratio decreased a little with the increase of Ni loading. This means that the selectivity of two gases did not change abruptly.

Ni/CeSmO catalyst was prepared for ESR reaction by Rodrigues et al. [107]. They reported long term stability of the catalyst (192 h) for the reaction carried out at 550 °C (Fig. 6). Incorporation of Ni into ceria exhibits high oxygen vacancy and suppresses coke deposition over the catalyst surface. CO selectivity was quite high for Ni/CeSmO catalyst. So, the H_2/CO ratio was less.

Chemistry of ethanol steam reforming

There are several proposed mechanisms based on real ethanol conversion over different catalyst surfaces [115–119]. However, there is still no evidence for the actual reaction pathways due to complexity of large catalyst components and reaction conditions (temperature, steam to ethanol molar ratio and residence time). Generally, the reaction steps are:

Ethanol dehydrogenation to acetaldehyde (Eq. (5)).

Ethanol decomposition to CH_4, CO and H_2 (Eq. (6)).

Acetaldehyde decomposition to CH_4 and CO:

$$CH_3CHO \rightarrow CH_4 + CO$$

Methane steam reforming:

$$CH_4 + H_2O \rightarrow CO + 3H_2$$

Water gas shift reaction (Eq. (3)).

However, many other side reactions also occur based on properties of active metal and support, which results in the coke formation and less hydrogen yield [120–122]. The side reactions are stated below:

Ethanol dehydration to ethylene

$$C_2H_5OH \rightarrow H_2O + C_2H_4$$

Ethylene polymerization to coke (Eq. (11))

Production of acetone via acetaldehyde condensation, followed by decarboxylation:

$$2CH_3CHO \rightarrow CH_3COCH_3 + CO + H_2$$

Methane cracking (Eq. (13)).

Boudouard reaction (Eq. (12)).

Reverse of carbon gasification

$$CO + H_2 \rightarrow H_2O + C$$

Ethanol steam reforming (ESR) over Ni based catalysts is considered in this review basically due to their low cost. It

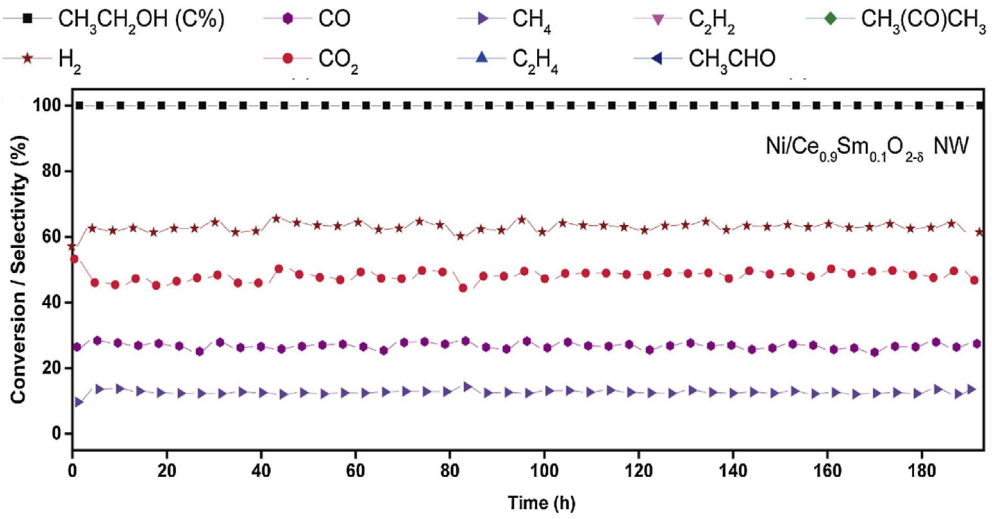

Fig. 6 – The time on stream study performed using $Ni/Ce_{0.9}Sm_{0.1}O_{2-\delta}$ nanowires as catalysts (Reaction conditions: 550 °C and H_2O/C_2H_5OH molar ratio = 3). Reprinted with permission from Ref. [107].

reduces the whole production cost of ESR process. The structure of Ni-based depends on preparation method and metal loading. Different Ni based catalysts activity are reported based on reaction conditions. The main drawback of Ni based catalyst is coke deposition during reforming process. Several strategies such as promoters and different supports are used to enhance the activity of the catalyst. ESR reaction mechanism is discussed.

Glycerol steam reforming

Very recently, GSR has become a very attractive topic compared to other processes such as auto-thermal reforming, partial oxidation gasification, aqueous-phase reforming and supercritical water reforming to produce H_2 [123]. In order to industrially adopt this process, it requires only feedstock change from natural gas or naphtha to glycerol [124]. However, several challenges are associated with GSR process. The main challenges are:

GSR is an endothermic process; so, it requires high temperature and consequently high operating cost. There are several side reactions that occur simultaneously in parallel with the main GSR reaction. These side reactions affect the product distribution and purity of hydrogen. Theoretically 7 mol hydrogen are produced per each mole of glycerol; many researchers reported an upper yield of hydrogen lower than 7 [125–127]. Although GSR is a thermodynamically controlled reaction, glycerol conversion depends on operating conditions, particularly at lower temperatures [128]. The formation of coke, during the GSR process, deactivates the catalyst. CO_2 generated along with H_2, is an environmental concern.

In order to overcome these challenges, new catalysts have been developed. Ni, Pt, Co and Ru based catalysts were investigated by many researchers for GSR [128]. Some others metal such as Rh, Ir and Pd were also used in this process [44]. However, all the noble metals are quite expensive.

Ni-based catalysts for GSR studies

Ni-based catalysts were broadly used for GSR studies. The textural properties of some of the Ni-based catalysts are presented in Table 5.

Senseni et al. [129] synthesized 15%Ni/Al_2O_3 catalyst by an impregnation method. The catalyst exhibits type IV isotherm with H_2–shaped hysteresis loop according to IUPAC classification. This type of shape confirmed the mesoporous nature of the material. The hysteresis loop revealed the spherical nature of the material consisting of nonuniform agglomerated particles. Ni-ATP catalyst was prepared by co-precipitation method [130]. The catalyst showed type III isotherm with H_3-type hysteresis loop based on IUPAC classification that was confirmed by the Wang et al. [140]. The volume of adsorbed N_2 at a relative pressure greater than 0.40 signifies the presence of appreciable mesoporous particles in the catalyst. The hysteresis loop confirmed that the material consists of aggregates of rod-like particles forming slitlike pores [141].

Ni and CeO_2 impregnated γ-Al_2O_3 catalysts were also prepared for GSR studies [131]. The surface area and pore volume decrease due to blockage of pores during impregnation of active metal and the modifier. Despite the reduction of surface area, the available area used for catalysis was in good agreements with the results of other researchers [142,143]. Ni/Al_2O_3 catalyst with varying Ni loading were tested in GSR [132]. Fig. 7 shows the pore size distribution and N_2 adsorption/desorption isotherms of Ni/Al_2O_3 catalysts with different Ni loading. Surface area and pore volume decreased with the increase of Ni loading. This is due to the partial collapse of Al_2O_3 pores with nickel oxide particles; which affects partially the mesoporous structure of the support [144]. The catalyst exhibits type IV isotherm and H_2 type hysteresis loop based on IUPAC classification (Fig. 7). This loop suggested that the mesoporous material contained agglomerated or interconnected particles with nonuniform pores [129,145].

Table 5 – Textural properties of different Ni-based catalysts.

Catalyst	Preparation method	S_{BET} (m^2/g)	Pore size (nm)	Pore Volume (cm^3/g)	Reference
$15Ni/Al_2O_3$	IMP	158.3	7.8	0.39	[129]
Ni-ATP	COP	140.6	7.65	0.38	[130]
$10Ni/Al_2O_3/5CeO_2$	WIMP	112	6.4	0.50	[131]
$10Ni/Al_2O_3$	WIMP	122	6.4	0.56	[131]
$10Ni/Al_2O_3/10CeO_2$	WIMP	104	6.6	0.49	[131]
Al_2O_3	–	188.3	8.1	0.66	[132]
$5Ni/Al_2O_3$	WIMP	183.5	8.75	0.53	[132]
$10Ni/Al_2O_3$	WIMP	176.6	8.0	0.47	[132]
$15Ni/Al_2O_3$	WIMP	158.3	7.8	0.39	[132]
$20Ni/Al_2O_3$	WIMP	143.3	7.4	0.36	[132]
$Ni/\gamma\text{-}Al_2O_3$	WIMP	160	12.4	0.60	[133]
$Ni/B_2O_3\text{-}Al_2O_3$	WIMP	192	9.2	0.53	[133]
$Ni/La_2O_3\text{-}Al_2O_3$	WIMP	83	16.1	0.37	[133]
$Ni/Al_2O_3\text{-}ZrO_2$	SG	234.9	2.330	0.2761	[134]
$Ni\text{-}Pd/Al_2O_3\text{-}ZrO_2$	SG	234.6	2.305	0.2719	[134]
$Ni\text{-}Pd/Al_2O_3\text{-}ZrO_2\text{-}La_2O_3$	SG	118.1	3.611	0.2174	[134]
Ni/Olivine	SG	5.861	16.89	0.04925	[134]
2.5% Ni/FA	WIMP	12.2	5.4	0.0114	[135]
5% Ni/FA	WIMP	11.4	5.3	0.0138	[135]
7.5% Ni/FA	WIMP	10.4	5.4	0.0141	[135]
10% Ni/FA	WIMP	9.0	5.2	0.019	[135]
$10\%Ni/30\%MgO\text{-}SiO_2\text{-}ET$	WIMP	136	–	–	[136]
$10\%Ni/30\%MgO\text{-}SiO_2\text{-}AC$	WIMP	72	–	–	[136]
$10\%Ni/30\%MgO\text{-}SiO_2\text{-}D$	PM	86	–	–	[136]
Ni/Al	WIMP	136	20.1	0.32	[137]
Ni/LaAl	WIMP	126	21.1	0.43	[137]
Ni/SBA-15	WIMP	545	8.3	0.91	[138]
Ni/Mg/SBA-15	WIMP	313	7.4	0.62	[138]
Ni/Ca/SBA-15	WIMP	291	7.3	0.58	[138]
10Ni-MCM-41	OPHM	824.6	3.78	0.84	[139]
$10Ni5TiO_2\text{-}MCM\text{-}41$	OPHM	787.3	3.78	0.82	[139]
$10Ni5CeO_2\text{-}MCM\text{-}41$	OPHM	716.3	3.65	0.75	[139]

IMP: Impregnation method, COP: co-precipitation method, WIMP: Weight impregnation method, SG: Sol-gel method, PM: Physical mixture method, OPHM: One-pot hydrothermal method.

As with Ni/Al_2O_3, the deposition of lanthanum oxide on the surface of $\gamma\text{-}Al_2O_3$ decreases the surface area due to sintering from calcination and blockage of some of the pores in alumina [133]. However, there was no significant change in surface area due to addition of B_2O_3. The structure of the support slightly deteriorates from the deposition of particles. Kousi et al. [133] concluded that the metal loading and calcination temperature were the main factors to obtain textural properties. Yurdakul et al. [134] prepared Ni based catalysts with different supports. The textural property of the catalyst changed after addition of La_2O_3. Surface area and pore volume decreased, but pore size increased. Olivine (a mineral used as fluidizing material in biomass gasifiers) supported catalyst showed less surface area compared to other catalysts. The pore size of the catalyst increased. Ni/flyash catalyst with different loadings of Ni were also used in GSR studies [135]. The surface area and pore volume decrease due to blockage of small pores with nickel particles. Pore diameter increases up to 7.5% Ni loading. However, when the loading was increased above 7.5%, the pore diameter decreased as Ni particle was adsorbed in the inner surface of the pore [146]. $Ni/Mg\text{-}SiO_2$ catalysts were synthesized with the help of two different solvents - ethanol and acetone [136]. The highest surface area was achieved with ethanol using an wet impregnation method. They reported that the increase in surface area was due to interaction of Ni with Mg and modifying the interaction between MgO and SiO_2. Thus, Ni particle dispersion increased. Different solvents used for preparation of catalysts changed the drying rate and solvent diffusion rate through the material pores. Ni/Al and Ni/LaAl catalysts were prepared by a wet impregnation method [137]. Surface area decreased with the modification of support with La. N_2 adsorption and desorption isotherms of catalysts exhibited same shape (type IV(a)). Minor adsorption of N_2 was observed at relatively lower pressure ($P/P^0 < 0.05$) and major adsorption occurred at higher pressure ($0.7 < P/P^0 < 1.0$) [147]. The type of isotherms indicated that the material was mesoporous. Ni/Al catalyst showed H_2(b) type hysteresis loop and other Ni/LaAl showed H_3 type hysteresis loop. Small hysteresis loop was observed in both cases due to desorption rate lower than adsorption rate (percolation effects on porous media) [148]. The BJH data showed that most of the population of pores were in the mesopore ranges. They observed that Ni/LaAl catalyst contained mainly meso, some macropores.

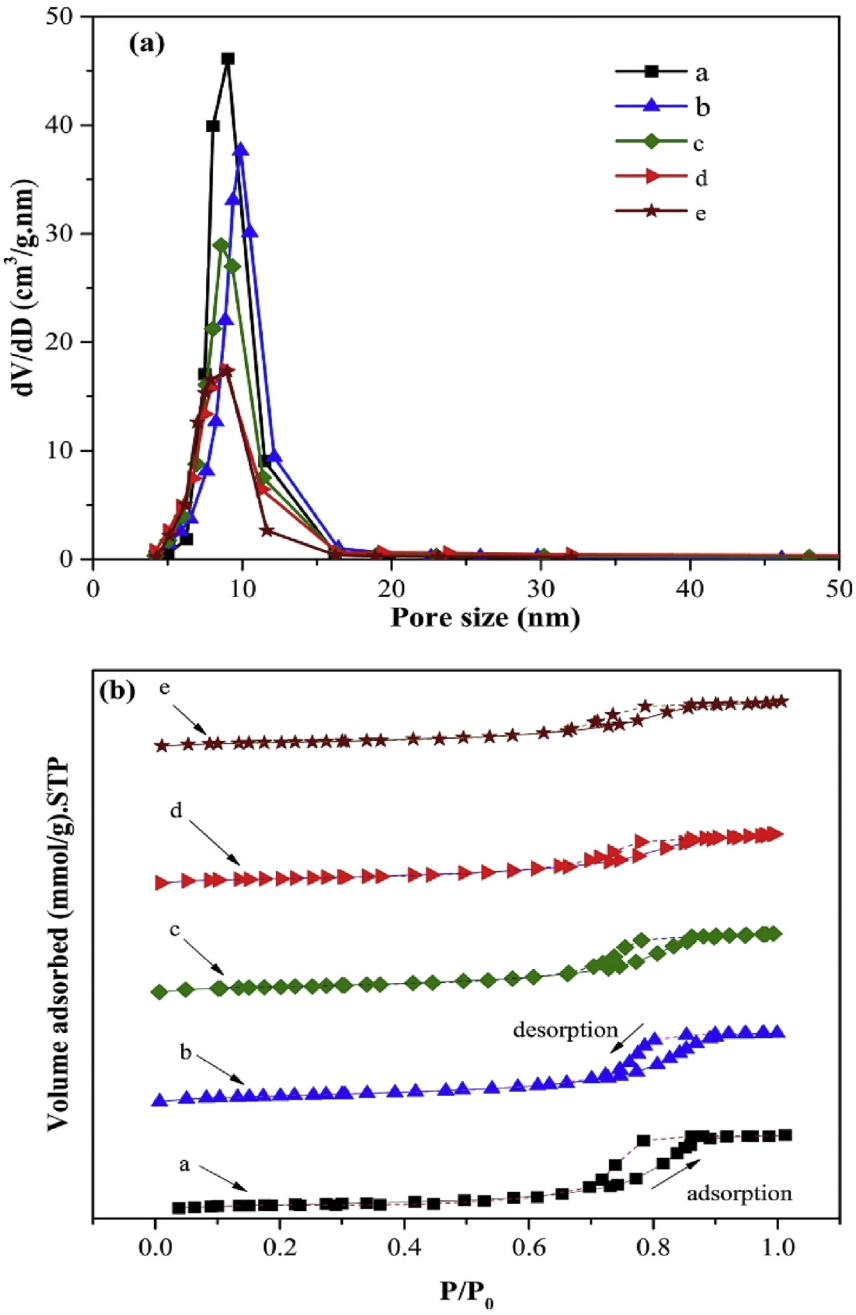

Fig. 7 – BET analysis plots: a) Pore size distributions and b) Nitrogen adsorption/desorption isotherms of XNi/Al_2O_3 catalysts calcined at 450 °C; a) Al_2O_3 Support, b) $5Ni/Al_2O_3$, c) $10Ni/Al_2O_3$, d) $15Ni/Al_2O_3$ and e) $20Ni/Al_2O_3$. Reprinted with permission from Ref. [132].

Calles et al. [138] prepared Ni on SBA-15 containing promoters (Mg and Ca) by wet impregnation method. N_2 adsorption-desorption isotherm showed that all the catalysts exhibit type IV isotherm with a hysteresis loop. The N_2 adsorbed volume decreases with the addition of Mg and Ca. This result suggests that there was loss of porosity due to incorporation of promoters. Ni-MCM-41 with the addition of Ce and Ti catalysts were synthesized by one pot hydrothermal synthesis method [139]. Surface area decreased with the increase of metal loading. This result indicates that incorporation of metallic oxides blocked the mesoporous matrix and decreased the average porosity. The pore size and pore volume were same after metal loading.

Activity of different nickel-based catalysts for glycerol steam reforming

Table 6 shows catalytic activity in terms of glycerol conversion and composition of gaseous products. Suffredini et al. [149] synthesized different Ni and Al based catalysts for GSR reaction. All the catalysts showed good results. H_2 and CO_2 were the major products of the main GSR reaction

Table 6 – GSR activity of Ni-based catalysts.

Catalyst	$X_{C_3H_8O_3}$ (%)	Temperature (°C)	S_{H_2} (%)/H_2 yield	S_{CO} (%)/CO yield	S_{CO_2} (%)/CO_2 yield	H_2/CO	Reference
Ni/Al_2O_3	99	600	69	6	24	11.5	[149]
$NiAl_2O_4$	99	600	67	9	24	7.44	[149]
$NiAl_2O_4/Al_2O_3$	99	600	70	6	24	11.67	[149]
$NiAl_2O_4+Al_2O_3$	99	600	68	7	24	9.71	[149]
NiLaCeZr	99.9	650	63.7	3.7	30.1	17.21	[150]
NiLaTi700	99.5	500	57.1	7.6	29.8	7.51	[151]
NiLaTi700	99.7	650	66.3	4.1	27.7	16.17	[151]
NiLaTi850	99.3	500	55.8	8.0	29.6	6.98	[151]
NiLaTi850	99.5	650	66.4	5.0	23.6	13.28	[151]
$Ni30CeO_2/C$	45	350	32	5.0	91	6.4	[152]
$NiSn30CeO_2/C$	52	350	48	28.0	65	1.71	[152]
Ni/Zr	90	600	65	60	60	1.08	[153]
Ni/SiZr	90	600	80	32	30	2.5	[153]
Ni/La_2O_3	70	650	68.3	3.5	27.7	19.51	[154]
Ni/Al_2O_3	80	650	75.1	8.3	12.6	9.05	[154]
Ni/ZrO_2	57	650	60.7	4.3	26.1	14.12	[154]
Ni/SiO_2	48	650	45.9	8.9	16.2	5.16	[154]
Ni/MgO	73	650	55.4	5.6	16.8	9.89	[154]
Ni/CeZrO-1	90.7	600	53.3	61.9	33	0.86	[155]
Ni/CeZrO-2	96.7	600	71.2	29.7	66.5	2.4	[155]
Ni/CeZrO-3	97.9	600	76.3	28.2	68.6	2.71	[155]
Ni/CeZrO-4	97.4	600	73.9	25.3	71.8	2.92	[155]
Ni/SBA-15	46.0	600	52.6	24.0	22.4	2.19	[138]
Ni/Mg/SBA-15	97.5	600	53.2	15.0	30.1	3.55	[138]
Ni/Ca/SBA-15	98.4	600	53.0	16.3	28.9	3.25	[138]
10Ni-MCM-41	91.9	650	81.0	21.5	71.4	3.77	[139]
$10Ni5TiO_2$-MCM-41	98.9	650	86.0	18.0	78.5	4.78	[139]
$10Ni5CeO_2$-MCM-41	97.3	650	88.4	25.4	71.6	3.48	[139]

(Eq. (8)). All the catalysts deactivated slowly due to carbon deposition over the catalyst surface. $NiAl_2O_4$ catalyst showed long term stability during GSR due to less carbon deposition (8.8%) on the surface. They also observed that Ni^0 particle size was an important factor for carbon deposition. Large particle size played a role on the initiation step via nucleation-growth mechanism [156]. $NiAl_2O_4/Al_2O_3$ catalyst yielded the highest value of H_2/CO ratio. This was due to high production of H_2 and less production of CO compared to other catalysts.

NiLaCeZr catalyst was also prepared for glycerol steam reforming reaction [150]. The catalyst showed good catalytic activity in terms of glycerol conversion and H_2 yield. The catalyst also showed good stability with respect of carbon removal from the active sites due to high basicity and the smaller size of nickel crystal. High basicity of the catalyst involved higher amount of oxygen vacancies which improved catalyst stability against sintering and coking [155,157]. The lower amount of CO was produced for NiLaCeZr. So, the H_2/CO ratio increased.

NiLaTi catalyst was prepared by Veiga et al. [151] at two different calcination temperature (700 °C and 850 °C). Both the catalysts showed high glycerol conversion. NiLaTi700 showed low carbon deposition, suggesting that this catalyst promotes coke gasification involving H_2O, CO_2 and lattice oxygen. Catalyst also contained small size nickel particles with permissible discernible activity. There was stronger interaction between Ni and other two metal oxides in NiLaAl700. This also contributed to good catalytic performance in GSR. Many researchers found that La_2O_3 facilitated Ni dispersion and increased the basic sites of the support [137,158,159]. Stronger interaction between active metals Ni and Ti prevented the catalyst from sintering and improved stability during steam reforming reactions [160]. Another catalyst NiLaTi850 containing $LaTiO_3$ perovskite with oxygen vacancies, improved mobility of lattice oxygen and increased interaction with carbon formed over Ni particles [161]. NiTi700 catalyst showed the highest H_2/CO ratio among all the catalysts. The CO yield was found less compared to other catalyst at higher temperature.

$Ni30CeO_2/C$ and $NiSn30CeO_2/C$ catalysts were also tested for GSR [152]. The composition of product gases varied due to addition of tin and is independent of ceria content (Fig. 8). $NiSn30CeO_2/C$ catalyst showed good activity in terms of H_2 yield (48%). This possibly happened due to interaction between Ni and Sn, resulting in the formation of Ni-Sn on the surface. Ni_3Sn alloy formed and maintained the high rates of C-C cleavage; needed for H_2 production [162]. $NiSn30CeO_2/C$ catalyst gave good stable performance due to presence of accessible reduced Ni and Sn^0. So, the synergistic effect influenced catalyst performance. 30% CeO_2 also provides higher number of accessible active sites. Upon addition of Sn in the catalyst, CO production increased. So, the H_2/CO ratio was reduced.

Ni/Zr and Ni/SiZr catalysts were synthesized by Charisiou et al. [153]. Addition of Si on the support influenced the distribution of product gases and mainly increased H_2 production and not favored reverse the water gas shift reaction (CO_2 to CO). So, the selectivity of CO decreased. Ni with different support catalysts were used in GSR [129]. The small Ni particle favored formation of CH_4 [163]. H_2/CO ratio increased a little due to addition of Si at 600 °C.

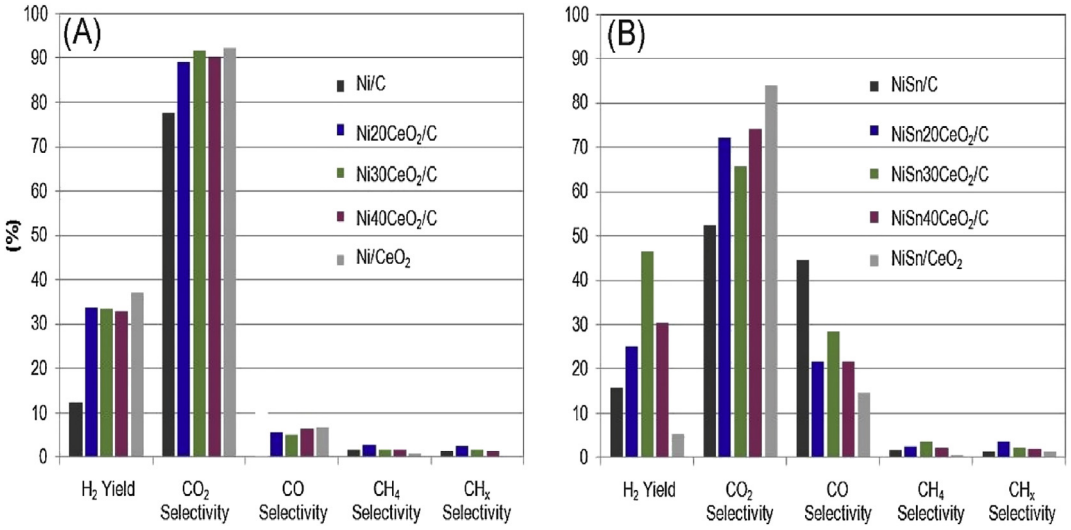

Fig. 8 – H_2 yield and selectivity of other gases produced in the GSR at 350 °C: $NiCeO_2$/C (A); $NiSnCeO_2$/C (B) Reprinted with permission from Ref. [152].

Zamzuri et al. [154] observed that the crystal size of Ni/La_2O_3 catalyst was large and it showed good activity during the reaction. Dehydration of glycerol to ethylene takes place over the surface of SiO_2, ZrO_2 and MgO supported catalyst. Ethylene subsequently produced coke (Equation (11)). So, the catalysts were deactivated within the operating conditions studied. Ni/Al_2O_3 and Ni/La_2O_3 catalysts were active enough to favor methane steam reforming and water gas shift reaction. Ni/Al_2O_3 catalyst showed good glycerol conversion and H_2 selectivity among all catalysts studied. Ni/La_2O_3 catalyst gave the highest value of H_2/CO ratio compared to other supported catalyst. This reflects that this catalyst selectively produced less amount of CO.

Ni/CeZrO catalyst with varying Ce loading influenced the product gas distribution [155]. The glycerol conversion and H_2 selectivity increased with the increase of Ce loading. Cerium content favored nickel dispersion over the catalyst support. They reported Ni/CeZrO-3 catalyst contained higher Ni active sites due to higher dispersion of Ni. Thus, this catalyst exhibited good activity [164]. CO selectivity decreases with increase of Ce content; which favors the water gas shift reaction. Water gas shift reaction occurred because cerium oxide enhances dissociation of H_2O and influenced reaction between steam and the adsorbed materials on the nickel catalyst [165,166]. Fig. 9 shows the time on stream behavior of the catalysts in terms of glycerol conversion and selectivity of product gases. Among all the catalysts, Ni/CeZrO-3 catalyst showed good catalytic activity. Glycerol conversion was stable with this catalyst up to 700 min. All catalysts except Ni/CeZrO-1 showed almost same H_2/CO ratio. Ni/CeZrO-1 catalyst produced more CO than H_2.

GSR reaction was also performed with mesoporous silica supports. Ni/SBA-15 modified with Mg and Ca was prepared and their activities were studied at 600 °C [138]. Ni/Ca/SBA-15 catalyst showed good catalytic activity in terms of glycerol conversion. Nickel dispersion increased with the incorporation of Mg and Ca and it affects the catalytic activity. Glycerol conversion decreased after 5 h for Ni/SBA-15 due to deactivation. However, Ni/Mg/SBA-15 and Ni/Ca/SBA-15 maintained high conversion (>95%), which reflects higher thermal stability due to metal support interaction. After addition of Mg and Ca, CO production was reduced for Ni/SBA-15 catalyst. So, H_2/CO ratio increased for Mg and Ca containing catalyst.

Ni-MCM-41 and promoted catalysts were also used for GSR studies in the temperature range of 450–700 °C [139]. Abrokwah et al. [139] obtained 650 °C as the optimum reaction temperature for these studies. H_2 selectivity increased with temperature and attained maximum at 650 °C. Modification of support with Ce and Ti increased H_2 selectivity as well as glycerol conversion. The authors concluded that the metal support interaction enhanced metal dispersion and could be the main factor to increase H_2 selectivity in these reactions. 10Ni5TiO_2-MCM-41 catalyst exhibits the highest value of H_2/CO ratio compared to other catalysts. This was due to less amount of CO production.

Chemistry of glycerol steam reforming

The overall glycerol steam reforming reaction (Eq. (8)) is endothermic and it is the combination of glycerol decomposition (Eq. (9)) and water gas shift reaction (Eq. (3)) [167]. The product distribution basically depends on the reaction conditions and the catalyst used. The CO is produced from glycerol decomposition which may further react with water to form CO_2 and H_2 via water gas shift reaction. In addition, methane formation can proceed by hydrogenation of CO or CO_2 and both of them are exothermic reactions [168].

$$CO + 3H_2 \leftrightarrow CH_4 + H_2O$$

$$CO_2 + 4H_2 \leftrightarrow CH_4 + 2H_2O$$

For high production of H_2 through glycerol steam reforming, the catalyst must work on cleavage of C-C, O-H and C-H bonds in the oxygenated hydrocarbons and should favor the

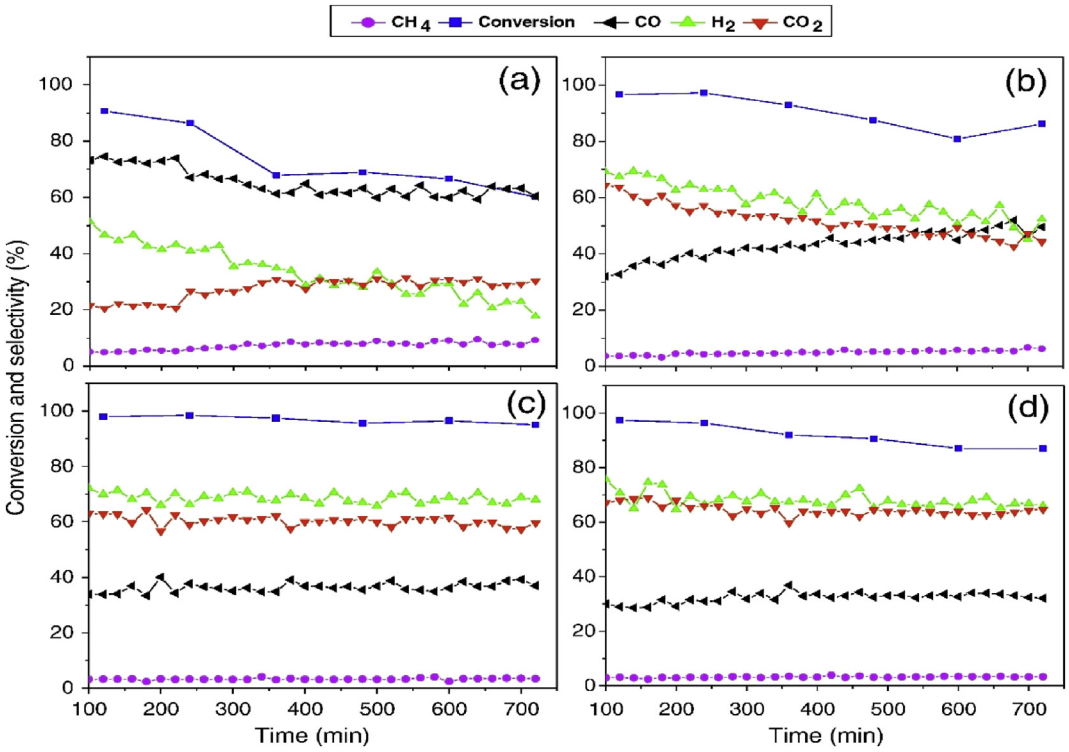

Fig. 9 – Glycerol conversion and gaseous product selectivity over Ni supported catalysts: (a) Ni/CeZrO-1; (b) Ni/CeZrO-2; (c) Ni/CeZrO-3 and (d) Ni/CeZrO-4 (Reaction conditions: 1 atm, 600 °C, FFR 0.06 ml/min, H_2O/glycerol molar ratio 24, N_2 carrier gas 33 ml/min). Reprinted with permission from Ref. [155].

water gas shift reaction to remove CO from catalyst surface as CO_2 [169].

Many noble (Rh, Pt, Ru) and non-noble metals (Co, Ni) are used in glycerol steam reforming (GSR) reaction. Among non-noble metals, Ni based catalysts are generally used for GSR. The effect of preparation method, metal loading and different support on the catalyst structure is discussed. Catalyst activity based on reaction temperature and metal loading is reported. GSR reaction mechanism is also discussed.

Discussions

In summary, Ni based catalysts have shown good catalytic behavior in steam reforming of methanol, ethanol and glycerol. Generally, Cu based catalysts are suitable for methanol steam reforming. However, some researchers developed Ni based catalysts for MSR. These catalysts gave promising catalytic activity in terms of methanol conversion and desired product distribution. In order to obtain high methanol conversion and desired products, researchers modified Ni catalysts with other noble metals and used different supports. Some side reactions also occur with the main methanol steam reforming reaction. These reactions can be suppressed through catalyst activity and reaction conditions. Development of suitable catalysts is still facing major challenges in the field of MSR reaction.

Ethanol steam reforming is more complicated than MSR. Several simultaneous side reactions occur during the main reaction. In ESR also, catalyst activity and reaction conditions are the main controlling parameters to reduce the side products. Coke formation over the catalyst surface is the main drawback in ESR. The active metal is needed to act on C-C cleavage of ethanol and to stop polymerization of intermediate products during ESR. Ni is the best suitable metal compared to other non-noble metals to act on C-C cleavage of ethanol. Decreasing the rate of coke production, increases the catalyst lifetime. Modification of catalyst by modifying metal, support and both are the key to reduce coke formation and can increase ethanol conversion and desired product distribution.

GSR is also complicated like ESR and MSR. The GSR reaction mainly occurs at higher temperature. Glycerol can be easily decomposed to form CO, CO_2, olefins, water hydrogen and oxygenates to reach the catalytic surface [170]. So, metal to activate C-O (typical of oxygenated compounds), C-C and C=C bonds to take consideration for the development of suitable catalysts. Ni is the suitable metal to work on the cleavage of C-C bond. Modification of Ni with different supports and other metals increased the catalytic activity. This also helped to reduce coke formation during GSR.

Conclusions

In the 21st century, hydrogen is a very promising energy carrier. It has major applications in different fields. Production of hydrogen from non-renewable resources (natural gas, naphtha, coal etc.) is currently carried out in industry. However, the sustainability of these non-renewable sources

are major concerns of today. Steam reforming of alcohols with different noble and non-noble metals is a highly efficient sustainable process for hydrogen production. Ni-based catalysts have been used extensively due to its low cost compared to noble metals. In methanol steam reforming, catalysts with high stability, catalyst activity and suppression of carbon monoxide at low temperature are the main objectives. For Ni-based catalysts, researchers pursued different approaches to improve the catalyst activity. In addition to high surface area, small particle size and metal support interactions have strong influence on its catalytic activity. In ethanol steam reforming, most studies are based on catalyst and catalyst-support interactions. The main criteria of ESR is that active metal (Ni) should be able to break the C-C bond. Several supports -TiO_2, Al_2O_3, ZSM-5, SF (silicon fiber) and β-zeolite have been investigated to ensure active metal dispersion, stability, and participation in the ESR reactions. Like ESR, GSR is also a promising route to produce hydrogen. The choice of a good catalyst is important to enhance GSR performance for improved hydrogen production. Interaction between metal and support, metal loading and high surface area are basically important for the catalyst activity. Several approaches have been made for Ni-based catalysts to increase its performance. Different metal oxides such as ZrO_2, Al_2O_3, SiO_2, MgO and La_2O_3 have been studied as a support in GSR reactions. The main drawback of all the steam reforming reactions is the deactivation of the catalyst. Catalyst deactivation can be mainly classified into the following types: (i) coke formation; (ii) active metal sintering or oxidation. In order to overcome these problems, several strategies have been reported such as catalyst modification with promoter, small particle size, presence of lattice oxygen and increasing water to alcohol ratio of the reactions.

The main objective of this review is to concentrate on Ni based catalyst development which gives prominent activity and stability on three different steam reforming processes. Catalyst needs to be resistant to carbon deposition as well as sintering at higher reaction temperature. Combining reforming reactions can also be considered such as steam reforming with partial oxidation because heat released from partial oxidation can be used in endothermic steam reforming reactions. So, no external source of energy is required for this process.

The size of the catalyst particle is also responsible for catalyst activity in terms of reactants conversion and products yield. In order to increase the catalyst activity, further research can be focused on metal dispersion over high surface area containing amorphous materials. In addition, catalyst supports prepared from waste material can also be considered in steam reforming process.

Acknowledgements

This work was performed at North Carolina A&T State University. The authors acknowledge the support received from NSF CREST (#260326) and UNC-ROI (#110092). We thank Mr. Nafeezuddin Mohammad for his help with this review.

REFERENCES

[1] Sharma S, Ghoshal SK. Hydrogen the future transportation fuel: from production to applications. Renew Sustain Energy Rev 2015;43:1151–8.
[2] Mazloomi K, Gomes C. Hydrogen as an energy carrier: prospects and challenges. Renew Sustain Energy Rev 2012;16:3024–33.
[3] Schwengber CA, Alves HJ, Schaffner RA, Silva FA, Sequinel R, Bach VR, Ferracin RJ. Overview of glycerol reforming for hydrogen production. Renew Sustain Energy Rev 2016;58:259–66.
[4] Olah GA, Geoppert A, Surya Prakash GK. Beyond oil and gas: the methanol economy. 2nd ed. Germany: Wiley-VCH; 2009.
[5] Cecere D, Giacomazzi E, Ingenito A. A review on hydrogen industrial aerospace applications. Int J Hydrogen Energy 2014;39:10731–47.
[6] Lee DS, Pitari G, Grewe V, Gierens K, Penner JE, Petzold A, Prather MJ, Schumann U, Bais A, Berntsen T, Iachetti D, Lim LL, Sausen R. Transports impacts on atmosphere and climate: aviation. Atmos Environ 2010;44:4678–734.
[7] Taboada E, Angurell I, Llorca J. Dynamic photocatalytic hydrogen production from ethanol–water mixtures in an optical fiber honeycomb reactor loaded with Au/TiO_2. J Catal 2014;309:460–7.
[8] Ni M, Leung MKH, Leung DYC, Sumathy K. A review and recent developments in photocatalytic water-splitting using TiO_2 for hydrogen production. Renew Sustain Energy Rev 2007;11:401–25.
[9] Marone A, Izzo G, Mentuccia L, Massini G, Paganin P, Rosa S, Varrone C, Signorini A. Vegetable waste as substrate and source of suitable microflora for bio-hydrogen production. Renew Energy 2014;68:6–13.
[10] Gallucci F, Basile A. Palladium membrane reactor for steam reforming reaction: a comparison between deferent fuels. Int J Hydrogen Energy 2008;33:1671–87.
[11] Sun J, Qiu X, Wu F, Zhu W, Wang W, Hao S. Hydrogen from steam reforming of ethanol in low and middle temperature range for fuel cell application. Int J Hydrogen Energy 2004;29:1075–81.
[12] Ribeirinha P, Alves I, Vidal Vazquez F, Schuller G, Boaventura M, Mendes A. Heat integration of methanol steam reformer with a high-temperature polymeric electrolytic membrane cell. Energy 2017;120:468–71.
[13] Ribeirinha P, Abdollahzadeh M, Sousa JM, Boaventura M, Mendes A. Modelling of a high-temperature polymer electrolyte membrane fuel cell integrated with a methanol steam reformer cell. Appl Energy 2017;202:6–19.
[14] Sa S, Silva S, Brandao L, Sousa JM, Mendes A. Catalysts for methanol reforming-A review. Appl Catal B Environ 2010;99:43–57.
[15] Ewan BCR, Allen RWK. A figure of merit assessment of the routes to hydrogen. Int J Hydrogen Energy 2005;30:809–19.
[16] Basile A, Lulianelli A, Longo T, Liguori S, De FM. Pd-based selective membrane State-of-the Art [Chapter 2]. In: Marrwlli L, De Falco M, laquaniello G, editors. Membrane reactors for hydrogen production processes. Springer London Dordrecht Heidelberg New York; 2011. p. 21–55. ISBN 978-0-85729-150-9, https://doi.org/10.1007/978-0-85729-151-6.
[17] Ramirez D, Beites LF, Blazquez F, Ballesteros JC. Distributed generation system with PEM fuel cell for electrical power quality improvement. Int J Hydrogen Energy 2008;33:4433–43.
[18] Wee JH. Applications of proton exchange membrane fuel cell systems. Renew Sustain Energy Rev 2007;11:1720–38.

[19] Bose S, Kuila T, Nguyen TXH, Kim NH, Lau KT, Lee JH. Polymer membranes for high temperature proton exchange membrane fuel cell: recent advances and challenges. Prog Polym Sci 2011;36:813–43.
[20] Lulianelli A, Ribeirinha P, Mendes A, Basile A. Methanol Steam reforming for hydrogen generation via conventional and membrane reactors: a review. Renew Sustain Energy Rev 2014;29:355–68.
[21] Rifkin J. The hydrogen economy: the creation of the worldwide energy web and the redistribution of power on earth. Jeremy P. Tarcher, Penguin; 2002. ISBN 1-58542-193-6.
[22] Abrokwah RY, Deshmane VG, Kuila D. Comparative performance of M-MCM-41(M: Cu,Co,Ni,Pd,Zn and Sn) catalysts for steam reforming of methanol. J Mol Catal A Chem 2016;425:10–20.
[23] Rivarolo M, Bellotti D, Magistri L, Massardo AF. Feasibility study of methanol production from different renewable sources and thermo-economic analysis. Int J Hydrogen Energy 2016;41:2015–116.
[24] Rizza LS, Coronel CD, Smachetti MES, Nascimento MD, Curatti L. A semi-closed loop microalgal biomass production-platform for ethanol from renewable sources of nitrogen and phosporous. J Clean Prod 2019;219:217–24.
[25] Cai F, Lu P, Ibrahim JJ, Fu Y, Zhang J, Sun Y. Investigation of the role of Nb on Pd-Zr-Zn catalyst in methanol steam reforming for hydrogen production. Int J Hydrogen Energy 2019;44:11717–33.
[26] Telotte JC, Kern J, Palanki S. Miniaturized methanol reformer for fuel cell powered mobile applications. Int J Chem React Eng 2008;6:A64.
[27] Basile A, Parmaliana A, Tosti S, Lulianelli A, Gallucci F, Espro C, Spooren J. Hydrogen production by methanol steam reforming carried out in membrane reactor on Cu/Zn/Mg-based catalyst. Catal Today 2008;137:17–22.
[28] Zhang X, Hu H, Zhu Y, Zhu S. Methanol steam reforming to hydrogen in a carbon membrane reactor system. Ind Eng Chem Res 2006;45:7997–8001.
[29] Peppley BA, Amphlett JC, Kearns LM, Mann RF. Methanol-steam reforming on Cu/ZnO/Al2O3. Part 1: the reaction network. Appl Catal A 1999;179:21–9.
[30] Peppley BA, Amphlett JC, Kearns LM, Mann RF. Methanol-steam reforming on Cu/ZnO/Al2O3. Part 2: a comprehensive kinetic model. Appl Catal A 1999;179:31–49.
[31] Barroso MN, Gomez MF, Arrua LA, Abello MC. Co catalysts modified by rare earths (La, Ce or Pr) for hydrogen production from ethanol. Int J Hydrogen Energy 2014;39:8712–9.
[32] Augusto BL, Costa LOO, Noronha FB, Colman RC, Mattos LV. Ethanol reforming over Ni/CeGd catalysts with low Ni content. Int J Hydrogen Energy 2012;37:12258–70.
[33] Vaidya PD, Rodrigues AE. Insight into steam reforming of ethanol to produce hydrogen for fuel cells. Chem Eng J 2006;117:39–49.
[34] Wu YJ, Alvarado FD, Santos JC, Gracia F, Cunha AF, Rodrigues AE. Sorption-enhanced steam reforming of ethanol: thermodynamic comparison of CO_2 sorbents. Chem Eng Technol 2012;35:847–58.
[35] Vaidya PD, Rodrigues AE. Kinetics of steam reforming of ethanol over Ru/Al_2O_3 catalyst. Ind Eng Chem Res 2006;32:3238–47.
[36] Haryanto A, Fernando S, Murali N, Adhikari S. Current status of hydrogen production techniques by steam reforming of ethanol: a review. Energy Fuels 2005;19:2098–106.
[37] Ni M, Leung DYC, Leung MKH. A review on reforming bio-ethanol for hydrogen production. Int J Hydrogen Energy 2007;32:3238–47.
[38] Zhou C-H, Beltramini JN, Fan YX, Lu GQ. Chemoselective catalytic conversion of glycerol as a biorenewable source to valuable commodity chemicals. Chem Soc Rev 2007;37:527–49.
[39] Dou B, Song Y, Wang C, Chen H, Xu Y. Hydrogen production from catalytic steam reforming of biodiesel byproduct glycerol: issues and challenges. Renew Sustain Energy Rev 2014;30:950–60.
[40] Rahmat N, Abdullah AZ, Mohamed AR. Recent progress on innovative and potential technologies for glycerol transformation into fuel additives: a critical review. Renew Sustain Energy Rev 2010;14:987–1000.
[41] Wu G, Zhang C, Li S, Han Z, Wang T, Ma X, Gong J. Hydrogen production via glycerol steam reforming over Ni/Al_2O_3: influence of Nickel Precursors. ACS Sustainable Chem Eng 2013;1:1052–62.
[42] Mattos LV, Jacobs G, Davis BH, Noronha FB. Production of hydrogen from ethanol: review of reaction mechanism and catalyst deactivation. Chem Rev 2012;112:4094–123.
[43] Hou T, Zhang S, Chen Y, Wang D, Cai W. Hydrogen production from ethanol reforming: catalysts and reaction mechanism. Renew Sustain Energy Rev 2015;44:132–48.
[44] Adhikari S, Fernando S, Gwaltney SR, Filipto SD, Bricka PM, Steele PH, Haryanto A. A thermodynamic analysis of hydrogen production by steam reforming of glycerol. Int J Hydrogen Energy 2007;32:2875–80.
[45] Yaws CL. Chemical Process Handbook: physical, thermodynamic, environmental, transport, safety and health related properties for organic and inorganic chemicals. New York: McGraw-Hill; 1999.
[46] Fierro V, Klouz V, Akdim O, Mirodatos C. Oxidative reforming of biomass derived ethanol for hydrogen production in fuel cell applications. Catal Today 2002;75:141–4.
[47] Adhikari S, Fernando S, Haryanto A. Production of hydrogen by steam reforming of glycerin over alumina-supported metal catalysts. Catal Today 2007;129:355–64.
[48] Zhang B, Tang X, Li Y, Xu Y, Shen W. Hydrogen production from steam reforming of ethanol and glycerol over ceria-supported metal catalysts. Int J Hydrogen Energy 2011;36:2367–73.
[49] Bobadilla LF, Palma S, Ivanova S, Dominguez MI, Romero-Sarria F, Centeno MA, Odriozola JA. Steam reforming of methanol over supported Ni and Ni-Sn nanoparticles. Int J Hydrogen Energy 2013;38:6646–56.
[50] Gamba O, Moreno S, Molina R. Catalytic performance of Ni-Pr supported on delaminated clay in the dry reforming of methane. Int J Hydrogen Energy 2011;36:1540–50.
[51] Daza CE, Gallego J, Mondragon F, Moreno S, Molina R. High Stability of Ce-promoted Ni/Mg-Al catalysts derived from hydrotalcites in dry reforming of methane. Fuel 2010;89:592–603.
[52] Lytkina AA, Orekhova NV, Ermilova MM, Belenov SV, Guterman VE, Efimov MN, Yaroslavtsev AB. Bimetallic Carbon nanocatalysts for methanol steam reforming in conventional and membrane reactors. Catal Today 2016;268:60–7.
[53] Kim W, Mohaideen KK, Seo DJ, Yoon WL. Methanol-steam reforming reaction over Cu-Al-based catalysts derived from layered double hydroxides. Int J Hydrogen Energy 2017;42:2081–7.
[54] Lu J, Li X, He S, Han C, Wan G, Lei Y, Chen R, Liu P, Chen K, Zhang L, Luo Y. Hydrogen production via methanol steam reforming over Ni-based catalysts: influences of Lanthanum (La) addition and supports. Int J Hydrogen Energy 2017;42:3647–57.
[55] Ma Y, Guan G, Shi C, Zhu A, Hao X, Wang Z, Kusakabe K, Abudula A. Low-temperature steam reforming of methanol to produce hydrogen over various metal-doped molybdenum carbide catalysts. Int J Hydrogen Energy 2014;39:258–66.

[56] Tahay P, Khani Y, Jabari M, Bahadoran F, Safari N. Highly porous monolith/TiO_2 supported Cu, Cu-Ni, Ru and Pt catalysts in methanol steam reforming process for H_2 generation. Appl Catal A 2018;554:44–53.
[57] Deshmane VG, Owen SL, Abrokwah RY, Kuila D. Mesoporous nanocrystalline TiO_2 supported metal (Cu, Co, Ni, Pd, Zn and Sn) catalysts: effect of metal-support interactions on steam reforming of methanol. J Mol Catal A Chem 2015;408:202–13.
[58] Qi C, Amphlett JC, Peppley BA. Methanol steam reforming over NiAl and Ni (M) Al layered double hydroxides (M= Au, Rh, Ir) derived catalysts. Catal Lett 2005;104:57–62.
[59] Rogatis LD, Montini T, Lorenzut B, Fornasiero P. Ni_xCu_y/Al_2O_3 based catalysts for hydrogen production. Energy Environ Sci 2008;1:405–12.
[60] Liu Z, Yao S, Johnston-Peck A, Xu W, Rodriguez JA, Senanayake SD. Methanol steam reforming over Ni-CeO_2 model and powder catalysts: pathways to high stability and selectivity for H_2/CO_2 production. Catal Today 2018;311:74–80.
[61] Khzouz M, Gkanas EI, Du S, Wood J. Catalytic performance of Ni-Cu/Al_2O_3 for effective syngas production by methanol steam reforming. Fuel 2018;232:672–83.
[62] Men Y, Yang M. SMSI-like behavior and Ni promotion effect on NiZnAl catalysts in steam reforming of methanol. Catal Commun 2012;22:68–73.
[63] Barton J, Pour V. Kinetics of catalytic conversion of methanol at high pressures. Collect Czechoslov Chem Commun 1980;45:3402–7.
[64] Santacesaria E, Carra S. Kinetics of catalytic steam reforming of methanol in a CSTR reactor. Appl Catal 1983;5:345–58.
[65] Amphlett JC, Evans MJ, Mann RF, Weir RD. Hydrogen production by the catalytic steam reforming of methanol: Part 2: kinetics of methanol decomposition using girdler G66B catalyst. Can J Chem Eng 1985;63:605–11.
[66] Pour V, Barton J, Benda A. Kinetics of catalyzed reaction of methanol with water vapour. Collect Czechoslov Chem Commun 1975;40:2923–34.
[67] Takahashi K, Takezawa N, Kobayashi H. The mechanism of steam reforming of methanol over a copper-silica catalyst. Appl Catal 1982;2:363–6.
[68] Peppley BA, Amphlett JC, Kearns LM, Mann RF. Methanol–steam reforming on Cu/ZnO/Al_2O_3 catalysts. Part 2. A comprehensive kinetic model. Appl Catal A 1999;179:31–49.
[69] Pereira EB, Piscina PRdL, Marti S, Homs N. H_2 production by oxidative steam reforming of ethanol over K promoted Co-Rh/CeO_2-ZrO_2 catalysts. Energy Environ Sci 2010;3:487–93.
[70] Han X, Yu Y, He H, Shan W. Hydrogen production from oxidative steam reforming of ethanol over rhodium catalysts supported on Ce-La solid solution. Int J Hydrogen Energy 2013;38:10293–304.
[71] Costa LOO, Vasconcelos SMR, Pinto AL, Silva AM, Mattos LV, Noronha FB, Borges LEP. Rh/CeO_2 catalyst preparation and characterization for hydrogen production from ethanol partial oxidation. J Mater Sci 2008;43:440–9.
[72] Kraleva E, Sokolov S, Nasillo G, Bentrup U, Ehrich H. Catalytic performance of CoAlZn and NiAlZn mixed oxides in hydrogen production by bio-ethanol partial oxidation. Int J Hydrogen Energy 2014;39:209–20.
[73] Beyhan S, Legar JM, Kadirgan F. Understanding the influence of Ni, Co, Rh and Pd addition to PtSn/C catalyst for the oxidation of ethanol by in situ fourier transform infrared spectroscopy. Appl Catal, B 2014;144:66–74.
[74] Chen HQ, Yu H, Yang GX, Peng F, Wang HJ, Wang J. Auto-thermal ethanol micro-reformer with a structural Ir/La_2O_3/ZrO_2 catalyst for hydrogen production. Chem Eng J 2011;167:322–7.
[75] Silva AM, Costa LOO, Barandas APMG, Borges LEP, Mattos LV, Noronha FB. Effect of the metal nature on the reaction mechanism of the partial oxidation of ethanol over CeO_2-supported Pt and Rh catalysts. Catal Today 2008;133–135:755–61.
[76] He Z, Yang M, Wang XQ, Zhao Z, Duan AJ. Effect of the transition metal oxide supports on hydrogen production from bio-ethanol reforming. Catal Today 2012;194:2–8.
[77] Shejale AD, Yadav GD. Cu promoted Ni-Co/hydrotalcite catalyst for improved hydrogen production in comparison with several modified Ni-based catalysts via steam reforming of ethanol. Int J Hydrogen Energy 2017;42:11321–32.
[78] Han SJ, Song JH, Bang Y, Yoo J, Park S, Kang KH, Song IK. Hydrogen production by steam reforming of ethanol over mesoporous Cu-Ni-Al_2O_3-ZrO_2 xerogel catalysts. Int J Hydrogen Energy 2016;41:2554–63.
[79] Eigen M. Fast elementary steps in chemical reaction mechanisms. Pure Appl Chem 1963;6:97–116.
[80] Kruger H. Techniques for kinetic study of fast reactions in solution. Chem Soc Rev 1982;11:227–55.
[81] Han SJ, Bang Y, Song JH, Yoo J, Park S, Kang KH, Song IK. Hydrogen production by steam reforming of ethanol over dual-templated Ni-Al_2O_3 catalyst. Catal Today 2016;265:103–10.
[82] Bepari S, Basu S, Pradhan NC, Dalai AK. Steam reforming of ethanol over cerium-promoted Ni-Mg-Al hydrotalcite catalysts. Catal Today 2017;291:47–57.
[83] Chiou JYZ, Kung H-Y, Wang C-B. Highly stable and active Ni-doped ordered mesoporous carbon catalyst on the steam reforming of ethanol production. J Saudi Chem Soc 2017;21:205–9.
[84] Ramirez-Hernandez GY, Viveros-Garcia T, Fuentes-Ramirez R, Galindo-Esquivel IR. Promoting behavior of yttrium over nickel supported on alumina-yttria catalysts in the ethanol steam reforming reaction. Int J Hydrogen Energy 2016;41:9332–43.
[85] Prasongthum N, Xiao R, Zhang H, Tsubaki N, Natewong P, Reubroycharoen P. Highly active and stable Ni supported on CNTs-SiO_2 fiber catalysts for steam reforming of ethanol. Fuel Process Technol 2017;160:185–95.
[86] Rodriguez-Gomez A, Caballero A. Bimetallic Ni-Co/SBA-15 catalysts for reforming of ethanol: how cobalt modifies the nickel metal phase and product distribution. Mol Catal 2018;449:122–30.
[87] Li M, Wang X, Li S, Wang S, Ma X. Hydrogen production from ethanol steam reforming over nickel based catalyst derived from Ni/Mg/Al hydrotalcite-like compounds. Int J Hydrogen Energy 2010;35:6699–708.
[88] Song JH, Han SJ, Yoo J, Park S, Kim DH, Song IK. Hydrogen production by steam reforming of ethanol over Ni-Sr-Al_2O_3-ZrO_2 aerogel catalyst. J Mol Catal A Chem 2016;424:342–50.
[89] Cavani F, Trifiro F, Vaccari A. Hydrotalcite-type anionic clays: preparation, properties and applications. Catal Today 1991;11:173–301.
[90] Leofanti G, Padovan M, Tozzola G, Venturelli B. Surface area and pore texture of catalysts. Catal Today 1998;41:207–19.
[91] Rivera JA, Fetter G, Jimenez Y, Xochipa MM, Bosch P. Nickel distribution in (Ni,Mg)/Al-layered double hydroxides. Appl Catal A 2007;316:207–11.
[92] Zhang J, Li F. Coke-resistant Ni@SiO_2 catalyst for dry reforming of methane. Appl Catal B Environ 2015;176–177:513–21.
[93] Klaigaew K, Samart C, Chaiya C, Yoneyama Y, Tsubaki N, Reubroycharoen P. Effect of preparation methods on

activation of cobalt catalyst supported on silica fiber for Fischer-Tropsch synthesis. Chem Eng J 2015;278:166–73.
[94] Karimi S, Tavasoli, Mortazavi Y, Karimi A. Cobalt supported on Graphene-a promising novel Fischer-Tropsch synthesis catalyst. Appl Catal A 2015;499:188–96.
[95] Rodriguez-Gomez A, Caballero A. Identification of outer and inner nickel particles in a mesoporous support: how the channels modify the reducibility of Ni/SBA-15 catalysts. ChemNanoMat 2017;3:94–7.
[96] Kong X, Zhu Y, Zheng H, Li X, Zhu Y, Li Y. Ni nanoparticles inlaid nickel phyllosilicate as a metal-acid bifunctional catalyst for low-temperature hydrogenolysis reactions. ACS Catal 2015;5:5914–20.
[97] Zhang C, Yue H, Huang Z, Li S, Wu G, Ma X, Gong J. Hydrogen production via steam reforming of ethanol on phyllosilicate-derived Ni/SiO_2: enhanced metal-support interaction and catalytic stability. ACS Sustainable Chem Eng 2012;1:161–73.
[98] Bang Y, Han SJ, Yoo J, Park S, Choi JH, Lee YJ, Song JH, Song IK. Int J Hydrogen Energy 2014;39:4909–16.
[99] Baumann TF, Gash AE, Chinn SC, Sawvel AM, Maxwell RS, Satcher JH. Synthesis of high-surface-area alumina aerogels without the use of alkoxide precursors. Chem Mater 2005;17:395–401.
[100] Kumar A, Prasad R, Sharma YC. Ethanol steam reforming study over ZSM-5 supported cobalt versus nickel catalyst for renewable hydrogen generation. Chin J Chem Eng 2018. https://doi.org/10.1016/j.cjche.2018.03.036.
[101] Aguero FN, Alonso JA, Fernandez-Diaz MT, Cadus LE. Ni-based catalysts obtained from perovskites oxides for ethanol steam reforming. J Fuel Chem Technol 2018;46:1332–41.
[102] Wang S, He B, Tian R, Sun C, Dai R, Li X, Wu X, An X, Xie X. Ni-hierarchical Beta zeolite catalysts were applied to ethanol steam reforming: effect of sol gel method on loading Ni and the role of hierarchical structure. Mol Catal 2018;453:64–73.
[103] Tahir M, Mulewa W, Amin NAS, Zakaria ZY. Thermodynamic and experimental analysis on ethanol steam reforming for hydrogen production over Ni-modified TiO_2/MMT nanoclay catalyst. Energy Conserv Manag 2017;154:25–37.
[104] Song JH, Yoo S, Yoo J, Park S, Gim MY, Kim TH, Song IK. Hydrogen production by steam reforming of ethanol over Ni/Al_2O_3-La_2O_3 xerogel catalysts. Mol Catal 2017;434:123–33.
[105] Hong W, Lijuan Z, Muzhaozi Y, Tingyu X, Yuan L. Steam reforming of ethanol over Ni/$Ce_{0.7}Pr_{0.3}O_2$. J Rare Earths 2012;30:670–5.
[106] Hernandez IP, Gochi-Ponce Y, Contreras Larios JL, Fernandez AM. Steam reforming of ethanol over nickel-tungsten catalyst. Int J Hydrogen Energy 2010;35:12098–104.
[107] Rodrigues TS, Moura ABLd, Silva Fae, Candido EG, Silva AGMd, Oliveira DCd, Quiroz J, Camargo PHC, Bergamaschi VS, Ferreira JC, Linardi M, Fonseca FC. Ni supported $Ce_{0.9}Sm_{0.1}O_{2-\delta}$ nanowires: an efficient catalyst for ethanol steam reforming for hydrogen production. Fuel 2019;237:1244–53.
[108] Cunha AF, Wu YJ, Diaz AFA, Santos JC, Vaidya PD, Rodrigues AE. Steam reforming of ethanol on a Ni/Al_2O_3 catalyst coupled with a hydrotalcite-like sorbent in a multilayer pattern for CO_2 uptake. Can J Chem Eng 2012;90:1514–26.
[109] Montero C, Oar-Arteta L, Remiro A, Arandia A, Bilbao J, Gayubo AG. Thermodynamic comparison between bio-oil and ethanol steam reforming. Int J Hydrogen Energy 2015;40:15963–71.
[110] Tahir M, Amin NS. Photocatalytic CO_2 reduction with H_2O vapors using montmorillonite/TiO_2 supported microchannel monolith photoreactor. Chem Eng J 2013;230:314–27.
[111] Alberton AL, Souza MMVM, Schmal M. Carbon formation and its influence on ethanol steam reforming over Ni/Al_2O_3 catalysts. Catal Today 2007;123:257–64.
[112] Vicente J, Erena J, Montero C, Azkoiti MJ, Bilbao J, Gayubo AG. Reaction pathway for ethanol steam reforming on a Ni/SiO_2 catalyst including coke formation. Int J Hydrogen Energy 2014;39:18820–34.
[113] Comas J, Marino F, Laborde M, Amadeo N. Bio-ethanol steam reforming on Ni/Al_2O_3 catalyst. Chem Eng J 2004;98:61–8.
[114] Llorca J, de la Piscina PR, Sales J, Homes N. Direct production of hydrogen from ethanolic aquous solutions over oxide catalysts. Chem Commun 2001:641–2.
[115] Ozkan US, Zhang L, Song H. Investigation of the reaction network in ethanol steam reforming over supported cobalt catalysts. Ind Eng Chem Res 2010;49:8984–9.
[116] Mattos LV, Noronha FB. Hydrogen production for fuel cell applications by ethanol partial oxidation on Pt/CeO_2 catalysts: the effect of the reaction conditions and reaction mechanism. J Catal 2005;233:453–63.
[117] Li M, Wu Z, Overbury SH. Surface structure dependence of selective oxidation of ethanol on faceted CeO_2 nanocrystals. J Catal 2013;306:164–76.
[118] Jacobs G, Keogh RA, Davis BH. Steam reforming of ethanol over Pt/ceria with co-fed hydrogen. J Catal 2007;245:326–37.
[119] Lima SM, Silva AM, Costa L, Graham UM, Jacobs G, Davis BH, Mattos LV, Noronha FB. Study of catalyst deactivation and reaction mechanism of steam reforming, partial oxidation, and oxidative steam reforming of ethanol over Co/CeO2catalyst. J Catal 2009;268:268–81.
[120] Idriss H, Kim KS, Barteau MA. Carbon–carbon bond formation via aldolization of acetaldehyde on single crystal and polycrystalline TiO_2 surfaces. J Catal 1993;139:119–33.
[121] Idriss H, Barteau MA. Selectivity and mechanism shifts in the reactions of acetaldehyde on oxidized and reduced TiO_2(0 0 1) surfaces. Catal Lett 1996;40:147–53.
[122] Nishiguchi T, Matsumoto T, Kanai H, Utani K, Matsumura Y, Shen W, Imamura S. Catalytic steam reforming of ethanol to produce hydrogen and acetone. Appl Catal A 2005;279:273–7.
[123] Silva JM, Soria MA, Madeira LM. Challenges and strategies for optimization of glycerol steam reforming process. Renew Sustain Energy Rev 2015;42:1187–213.
[124] Avasthi KS, Reddy RN, Patel S. Challenges in the production of hydrogen from glycerol-a biodiesel byproduct via steam reforming process. Process Eng 2013;51:423–9.
[125] Dave CD, Pant KK. Renewable hydrogen generation by steam reforming of glycerol over zirconia promoted ceria supported catalyst. Renew Energy 2011;36:3195–202.
[126] Dieuzeide ML, Iannibelli V, Jobbagy M, Amadeo N. Steam reforming of glycerol over Ni/Mg/γ-Al_2O_3 catalysts. Effect of calcination temperatures. Int J Hydrogen Energy 2012;37:14926–30.
[127] Dieuzeide ML, Jobbagy M, Amadeo N. Glycerol steam reforming over Ni/γ-Al_2O_3 catalysts, modified with Mg (II). Effect of Mg (II) content. Catal Today 2013;213:50–7.
[128] Wang C, Dou B, Chen H, Song Y, Xu Y, Du X, Luo T, Tan C. Hydrogen production from steam reforming of glycerol by Ni-Mg-Al based catalysts in a fixed-bed reactor. Chem Eng J 2013;220:133–42.
[129] Senseni AZ, Fattahi SMS, Rezaei M, Meshkani F. A comparative study of experimental investigation and response surface optimization of steam reforming of glycerol over nickel nano-catalysts. Int J Hydrogen Energy 2016;41:10178–92.

[130] Chen M, Zhou Z, Wang Y, Liang T, Li X, Yang Z, Chen M, Wang J. Effects of attapulgite-supported transition metals catalysts on glycerol steam reforming for hydrogen production. Int J Hydrogen Energy 2018;43:20451–64.
[131] Demsash HD, Mohan R. Steam reforming of glycerol to hydrogen over ceria promoted nickel-alumina catalysts. Int J Hydrogen Energy 2016;41:22732–42.
[132] Senseni AZ, Meshkani F, Rezaei M. Steam reforming of glycerol on mesoporous nanocrystalline Ni/Al_2O_3 catalysts for H2 production. Int J Hydrogen Energy 2016;41:20137–46.
[133] Kousi K, Chourdakis N, Matralis H, Kontarides D, Papadopoulou C, Verykios X. Glycerol steam reforming over modified Ni-based catalysts. Appl Catal A 2016;518:129–41.
[134] Yurdukul M, Ayas N, Bizkarra K, Doukkali ME, Cambra JF. Preparation of Ni-based catalysts to produce hydrogen from glycerol by steam reforming process. Int J Hydrogen Energy 2016;41:8084–91.
[135] Bepari S, Pradhan NC, Dalai AK. Selective production of hydrogen by steam reforming of glycerol over Ni/Fly ash catalyst. Catal Today 2017;291:36–46.
[136] Thyssen VV, Sartore DM, Assaf EM. Effect of preparation method on the performance of $Ni/MgO\text{-}SiO_2$ catalysts for glycerol steam reforming. J Energy Inst 2018. https://doi.org/10.1016/j.joei.2018.07.010.
[137] Charisiou ND, Siakavelas G, Papageridis KN, Baklavaridis A, Tzounis L, Polychoronopoulou K, Goula MA. Hydrogen production via glycerol steam reforming reaction over nickel supported on alumina and lanthanum-alumina catalysts. Int J Hydrogen Energy 2017;42:13039–60.
[138] Calles JA, Carrero A, Vizcaino AJ, Garcia-Moreno L. Hydrogen Production by glycerol steam reforming over SBA-15-supported nickel catalysts: effect of alkaline earth promoters on activity and stability. Catal Today 2014;227:198–206.
[139] Abrokwah RY, Dade W, Owen SL, Deshmane V, Rahman M, Kuila D. Effect of mesoporous supports on metals on steam reforming of alcohols [Chapter 6]. In: Nanda S, Sarangi PK, Vo D-VN, editors. Fuel processing and energy utilization. Taylor and Francis Chapman and Hall/CRC New York; 2019. p. 93–108. ISBN 978-1-13859-320-6.
[140] Wang YS, Chen MQ, Yang J, Liu SM, Yang ZL, Wang J, Liang T. Hydrogen production from steam reforming of acetic acid over Ni-Fe/palygorskite modified with cerium. Bioresources 2017;12:4830–53.
[141] Cao JL, Shao GS, Wang Y, Liu YQ, Yuan ZY. CuO catalysts supported on attapulgite clay for low-temperature CO oxidation. Catal Commun 2018;9:2555–9.
[142] Iriondo A, Barrio VL, Cambra JF, Arias PL, Guemez MB, Sanchez-Sanchez MC. Glycerol steam reforming over Ni catalysts supported on ceria and ceria-promoted alumina. Int J Hydrogen Energy 2010;35:11622–33.
[143] Regalbuto J. In: Regalbuto John R, editor. Catalyst preparation: science and engineering. Taylor and Francis; 2007 (CRC Press, 2015).
[144] Zhao A, Ying W, Zhang H, Ma H, Fang D. $Ni\text{-}Al_2O_3$ catalysts prepared by solution combustion method for syngas methanation. Catal Commun 2012;17:34–8.
[145] Rahmani S, Rezaei M, Meshkani F. Preparation of highly active nickel catalysts supported on mesoporous nanocrystalline $\gamma\text{-}Al_2O_3$ for CO_2 methanation. J Ind Eng Chem 2014;20:1346–52.
[146] Wang S, Zhang F, Cai Q, Zhu L, Luo Z. Steam reforming of acetic acid over coal ash supported Fe and Ni catalysts. Int J Hydrogen Energy 2015;40:11406–13.
[147] Sing KSW, Everett DH, Hall RAW, Moscou L, Pierotti RA, Rouquerol J, Siemieniewska T. Reporting physisorption data for gas/solid systems with special reference to the determination of surface area and porosity. IUPAC 1985;57:603–19.
[148] Rouquerol F, Rouquerol J, Sing K. Adsorption by powders and porous solids. France, Marseille: Academic Press; 1999.
[149] Suffredini DFP, Thyssen VV, Almeida PMMd, Gomes RS, Borges MC, Farias AMDd, Assaf EM, Fraga MA, Brandao ST. Renewable hydrogen from glycerol reforming over nickel aluminate-based catalysts. Catal Today 2017;289:96–104.
[150] Veiga S, Romero M, Faccio R, Segobia D, Duarte H, Apesteguia C, Bussi J. Hydrogen-rich gas production by steam and oxidative steam reforming of crude glycerol over Ni-La-Me mixed oxide catalysts (Me=Ce and/or Zr). Catal Today 2019. https://doi.org/10.1016/j.cattod.2019.02.008.
[151] Veiga S, Faccio R, Segobia D, Apesteguia C, Bussi J. Hydrogen production by crude glycerol steam reforming over Ni-La-Ti mixed oxide catalysts. Int J Hydrogen Energy 2017;42:30525–34.
[152] Pastor-Parez L, Sepulveda-Escribano A. Multicomponent $NiSnCeO_2/C$ catalysts for the low-temperature glycerol steam reforming. Appl Catal A 2017;529:118–26.
[153] Charisiou ND, Papageridis KN, Siakavelas G, Sebastian V, Hinder SJ, Baker MA, Polychoronopoulou K, Goula MA. The influence of SiO_2 doping on the Ni/ZrO_2 supported catalyst for hydrogen production through the glycerol steam reforming reaction. Catal Today 2019;319:206–19.
[154] Zamzuri NH, Mat R, Amin NAS, Talebian-Kiakalaieh A. Hydrogen production from catalytic steam reforming of glycerol over various supported nickel catalysts. Int J Hydrogen Energy 2017;42:9087–98.
[155] Shao S, Shi A-W, Liu C-L, Yang R-Z, Dong W-S. Hydrogen production from steam reforming of glycerol Ni/CeZrO catalysts. Fuel Process Technol 2014;125:1–7.
[156] Rostrup-Nielsen JR, Sehested J, Norskov J. Hydrogen and synthesis gas by steam reforming and CO_2 reforming. Adv Catal 2002;47:65–139.
[157] Nahar G, Dupont V. Hydrogen production from simple alkanes and oxygenated hydrocarbons over ceria-zirconia supported catalysts: Review. Renew Sustain Energy Rev 2014;32:777–96.
[158] Carrero A, Vizcaino A, Calles J, Garcia-Moreno L. Hydrogen production through glycerol steam reforming using Co catalysts supported on SBA-15 doped with Zr, Ce and La. J Energy Chem 2017;26:42–8.
[159] Siew KW, Lee HC, Gimbun J, Chin SY, Khan MR, Taufiq-Yap YH, Cheng CK. Syngas production from glycerol-dry (CO_2) reforming over La-promoted Ni/Al_2O_3 catalyst. Renew Energy 2015;74:441–7.
[160] Nichele V, Signoretto M, Menegazzo F, Rossetti I, Cruciani G. Hydrogen production by ethanol steam reforming: effect of the synthesis parameters on the activity of Ni/TiO_2 catalysts. Int J Hydrogen Energy 2014;39:4252–8.
[161] Pena MA, Fierro JL. Chemical structures and performance of perovskite oxides. Chem Rev 2001;101:1981–2018.
[162] Shabaker JW, Simonetti DA, Cortright RD, Dumesic JA. Sn-modified Ni catalysts for aquous-phase reforming: characterization and deactivation studies. J Catal 2005;231:67–76.
[163] Chen SQ, Liu Y. $LaFe_yNi_{1-y}O_3$ supported nickel catalysts used for steam reforming of ethanol. Int J Hydrogen Energy 2009;34(11):4735–46.
[164] Wu G, Li S, Zhang C, Wang T, Gong J. Glycerol steam reforming over perovskite-derived nickel-based catalysts. Appl Catal B Environ 2014;144:277–85.
[165] Zhuang Q, Qin Y, Chang L. Promoting effect of cerium oxide in supported nickel catalyst for hydrocarbon steam-reforming. Appl Catal 1991;70:1–8.
[166] Cui Y, Galvita V, Rihko-Struckmann L, Lorenz H, Sundmacher K. Steam reforming of glycerol: the

experimental activity of $La_{1-x}Ce_xNiO_3$ catalyst in comparison to the thermodynamic reaction equilibrium. Appl Catal B Environ 2009;90:29–37.
[167] Sad ME, Duarte HA, Vignatti Ch, Padro CL, Apesteguia CR. Steam reforming of glycerol: hydrogen production optimization. Int J Hydrogen Energy 2015;40:6097–106.
[168] Dauenhauer PJ, Salge JR, Schmidt LD. Renewable hydrogen by autothermal steam reforming of volatile carbohydrates. J Catal 2006;244:238–47.
[169] Alcala R, Mavrikakis M, Dumesic JA. DFT studies for cleavage of C-C and C-O bonds in surface species derived from ethanol on Pt (111). J Catal 2003;218:178–90.
[170] Chiodo V, Freni S, Galvagno A, Mondello N, Frusteri F. Catalytic features of Rh and Ni supported catalysts in the steam reforming of glycerol to produce hydrogen. Appl Catal 2010;381:1–7.